Article

Not peer-reviewed version

Production and Characterisation of Polyhydroxyalkanoates from Cocoa Mucilage Using a Wild-Type *Priestia aryabhattai* Strain

Jimmy Nuñez-Pérez , Osmar J. Cornejo-Lucero , Rosario C. Espín-Valladares , Pedro Barba , Hortensia M. Rodríguez Cabrera , José-Manuel Pais-Chanfrau *

Posted Date: 31 March 2026

doi: 10.20944/preprints202603.2393.v1

Keywords: polyhydroxyalkanoates; poly(3-hydroxybutyrate); *Priestia aryabhattai*; cocoa mucilage; agro-industrial waste valorisation; response surface methodology; central composite design; Sudan Black B; circular bioeconomy

 doi:10.20944/preprints202603.2393.v1

Article

Production and Characterisation of Polyhydroxyalkanoates from Cocoa Mucilage Using a Wild-Type *Priestia aryabhattai* Strain

Jimmy Núñez-Pérez [1], Osmar J. Cornejo-Lucero [2], Rosario C. Espin-Valladares [1], Pedro Barba [3], Hortensia M. Rodríguez Cabrera [4] and José-Manuel Pais-Chanfrau [1,*]

[1] School of Agro-Industrial Engineering, Universidad Técnica del Norte (UTN), Ibarra 100105, Imbabura, Ecuador

[2] Instituto de Microbiología, Colegio de Ciencias e Ingeniería, Universidad San Francisco de Quito (USFQ), Diego de Robles y Vía Interoceánica, Quito 170901, Ecuador

[3] School of Biotechnology, Universidad Técnica del Norte (UTN), Ibarra 100105, Imbabura, Ecuador

[4] Yachay Tech Medicinal Chemistry Research Group (MEDCHEM-YT), School of Chemical Sciences and Engineering, Yachay Tech University, Urcuquí 100115, Imbabura, Ecuador

* Correspondence: jmpais@utn.edu.ec

Abstract

The accumulation of petroleum-based plastics demands sustainable alternatives such as polyhydroxyalkanoates (PHAs), biodegradable polyesters synthesised by numerous prokaryotes. However, high feedstock costs limit their commercialisation. This study evaluated cocoa mucilage, an underutilised by-product of the Ecuadorian cacao sector, as a low-cost carbon source for PHA production by a wild-type strain isolated from cocoa fruit residues. Bacteria were recovered from cocoa mucilage and pod shell fractions, screened for PHA accumulation by Sudan Black B staining with UV–Vis spectrophotometric confirmation, and identified by 16S rRNA gene sequencing. A first report of a single PHA-positive isolate, designated as *Priestia aryabhattai* strain NBP01-UTN, was recovered from the cocoa shell surface. Fermentation conditions were optimised using response surface methodology with a central composite design evaluating temperature, pH and ammonium sulphate concentration. The fitted quadratic model was highly significant (R^2 = 0.978, p < 0.0001), indentifying that temperature and nitrogen limitation were the dominant factors. Optimal conditions (40 °C, pH 7.30, 0 g·L^{-1} $(NH_4)_2SO_4$) yielded 0.496 g·L^{-1} PHA at 24 h (productivity ≈ 20.7 mg·L^{-1}·h^{-1}). FTIR and DSC analyses provided converging evidence consistent with poly(3-hydroxybutyrate). These results demonstrate the feasibility of coupling a locally isolated wild-type strain with cocoa mucilage for bioplastic production within a circular bioeconomy framework.

Keywords: polyhydroxyalkanoates; poly(3-hydroxybutyrate); *Priestia aryabhattai*; cocoa mucilage; agro-industrial waste valorisation; response surface methodology; central composite design; Sudan Black B; circular bioeconomy

1. Introduction

The escalating accumulation of petroleum-based plastic waste in terrestrial and aquatic ecosystems constitutes one of the most pressing environmental challenges of the twenty-first century. Global plastics production reached approximately 400 million tonnes in 2022, with the vast majority derived from non-renewable fossil resources and characterised by negligible biodegradability [1]. The persistence of conventional plastics in the environment, their fragmentation into microplastics and nanoplastics, and the consequent threats to biodiversity and human health have prompted an urgent search for sustainable alternatives [2]. In this context, bioplastics—polymers produced from renewable biological sources that are inherently biodegradable—have attracted considerable

 doi:10.20944/preprints202603.2393.v1

scientific and industrial attention as a viable pathway towards mitigating the plastic pollution crisis [3].

Among the various kinds of bioplastics, polyhydroxyalkanoates (PHAs) occupy a particularly prominent position. PHAs are intracellular polyesters synthesised by a wide range of prokaryotic organisms, such as carbon and energy storage reserves under conditions of nutrient imbalance, typically excess carbon and limitation of nitrogen, phosphorus or oxygen [4,5]. These biopolymers exhibit remarkable biodegradability and biocompatibility, and their physicochemical properties—including thermoplasticity, piezoelectricity and variable crystallinity- can rival those of conventional petrochemical plastics such as polypropylene and polyethene [6]. Furthermore, PHAs are fully degradable in soil, freshwater and marine environments by naturally occurring microorganisms, yielding only carbon dioxide and water under aerobic conditions [7]. Despite these attractive features, the widespread commercialisation of PHAs remains constrained by production costs that are approximately four to five times higher than those of petrochemical plastics, primarily owing to the expense of purified carbon substrates and downstream processing [8,9].

A promising strategy to reduce PHA production costs involves utilising low-cost or negative-cost agro-industrial waste streams as fermentation substrates [10,11]. Agroindustrial residues are often rich in fermentable sugars, organic acids and other nutrients that can serve as suitable carbon sources for PHA-producing microorganisms. The valorisation of such waste streams not only reduces feedstock costs but also addresses waste management challenges within the framework of the circular bioeconomy [12]. A wide variety of agro-industrial by-products have been explored for PHA production, including dairy whey, sugarcane molasses, crude glycerol from biodiesel manufacturing, rice husks and various fruit-processing residues [11,13,14].

Cacao (*Theobroma cacao* L.) is one of the most economically significant tropical crops worldwide. Global cacao production in the 2023/2024 season was approximately 4.5 million tonnes, with processing yielding an estimated 24 million tonnes of total fruit biomass when the non-marketable fractions are included [15]. Ecuador is the largest cacao producer in Latin America and ranks among the top four globally, with an estimated output of 330,000–430,000 metric tonnes per year and a global share of approximately 10% [15]. The cacao industry generates substantial quantities of agro-industrial residues: only 21–23% of the fruit's weight corresponds to the commercially exploited beans, whilst the remaining fractions—pod husks (approximately 67%), mucilage (approximately 9%) and bean shells (approximately 2%)—are typically discarded [14]. These residues represent an underutilised resource with significant potential for biotechnological valorisation, including fermentation to produce bioethanol, organic acids, pectin, and biopolymers [16].

Cocoa mucilage, the viscous pulp surrounding the cacao beans, is of particular interest as a fermentation substrate due to its high content of reducing sugars (glucose, fructose and sucrose) and its acidic pH, which can favour the growth of certain bacterial species [16]. Although cocoa mucilage plays an essential role during the natural fermentation of cacao beans for chocolate production, the surplus generated during post-harvest processing is largely treated as waste. Its transformation into value-added bioproducts, such as PHAs, would not only reduce the environmental burden associated with its disposal but also add economic value to the cacao production chain, benefiting smallholder farmers who account for most producers in Ecuador and globally [17]

The selection of efficient PHA-producing microbial strains is a critical factor in the development of cost-effective bioprocesses. Numerous genera, including *Cupriavidus,* Pseudomonas, Halomonas and members of the former Bacillus sensu lato, have been reported as PHA accumulators [6,7]. In 2020, Gupta et al. [18] reclassified several *Bacillus* species into the newly proposed genus *Priestia*, including the former *Bacillus megaterium* and Bacillus aryabhattai. *Priestia megaterium* (formerly B. megaterium) is one of the most extensively studied PHA producers, with a well-characterised poly(3-hydroxybutyrate) (PHB) biosynthetic pathway [19]. Closely related species within the *Priestia* clade, including *P. aryabhattai* and *P. flexa*, have also been reported to accumulate PHAs, although considerably fewer studies have investigated their bioplastic-producing potential compared to *P. megaterium* [20,21]. Notably, members of the genus *Priestia* are Gram-positive organisms, which

 doi:10.20944/preprints202603.2393.v1

confers a significant advantage for biomedical applications owing to the absence of endotoxin (lipopolysaccharide) contamination inherent to Gram-negative producers [22].

Optimising fermentation parameters is essential to maximise PHA yields and productivity when utilising complex agro-industrial substrates. Response surface methodology (RSM), particularly through central composite designs (CCD), has been extensively employed for the systematic optimisation of PHA production processes, enabling the simultaneous evaluation of multiple interacting variables such as temperature, pH and nutrient concentrations [23,24]. This statistical approach is especially valuable when working with novel strain–substrate combinations, as it enables the identification of optimal operating regions with fewer experimental runs.

The reliable identification and characterisation of produced PHAs require complementary analytical techniques. Fourier-transform infrared spectroscopy (FTIR) enables the detection of characteristic functional groups of the polyester backbone, whilst differential thermal analysis (DTA) or differential scanning calorimetry (DSC) provides essential information on the thermal behaviour, melting temperature and crystallinity of the polymer [4,25]. Together, these techniques permit a preliminary assessment of the type and quality of the accumulated PHA.

Despite the growing body of literature on PHA production from agro-industrial residues, studies utilising cocoa mucilage as the sole carbon source for PHA biosynthesis remain remarkably scarce. To the best of the authors' knowledge, no previous report has described the isolation of a PHA-producing *Priestia aryabhattai* strain directly from cocoa fruit residues.

The present study, therefore, aimed to: (i) isolate and screen bacteria from cocoa fruit residues (shells, pulp and mucilage) for PHA production potential using Sudan Black B staining; (ii) identify the most promising isolate through 16S rRNA gene sequencing and molecular characterisation; (iii) prepare and characterise the physicochemical properties of cocoa mucilage as a fermentation substrate; (iv) optimise the submerged fermentation conditions (temperature, pH and nitrogen source concentration) for PHA production using RSM with a CCD; and (v) characterise the resulting polymer by FTIR and DTA. This work contributes to the valorisation of cocoa agro-industrial waste within a circular bioeconomy framework, demonstrating the feasibility of coupling a novel wild-type isolate with a locally abundant, low-cost substrate for bioplastic production.

2. Materials and Methods

2.1. Isolation and Screening of PHA-Producing Microorganisms from Cocoa Fruit Residues

2.1.1. Sample Collection and Preparation

Microorganisms were isolated from by-products of cacao fruit (*Theobroma cacao* L.) obtained from smallholder farms in the parish of Lita, Imbabura Province, Ecuador. Two distinct fractions of the cacao fruit were processed as sources of potential PHA-producing bacteria: the mucilage (pulp exudate) and the outer shell (pod husk). All isolation procedures were carried out in the laboratories of the *Universidad Técnica del Norte* (UTN), Ibarra, Ecuador (Figure 1).

For the preparation of mucilage samples, cacao pods were washed with chlorinated water (100 $mg \cdot L^{-1}$ available chlorine) and rinsed with potable water to reduce surface contamination. The fruits were then sectioned transversely, and the beans were manually separated from the shell. The mucilaginous pulp surrounding the beans was extracted by pressing through a sterile cotton cloth, yielding approximately 1 L of raw mucilage per batch. When immediate processing was not feasible, samples were stored at 4 ± 1 °C for no longer than 24 h to minimise uncontrolled microbial proliferation. The collected mucilage samples were divided into aliquots and allowed to undergo spontaneous fermentation at ambient temperature (~25 °C) for 24, 48, and 72 h. After each fermentation period, 10 mL sub-samples were withdrawn and serially diluted in sterile distilled water from 10^{-1} to 10^{-6}.

 doi:10.20944/preprints202603.2393.v1

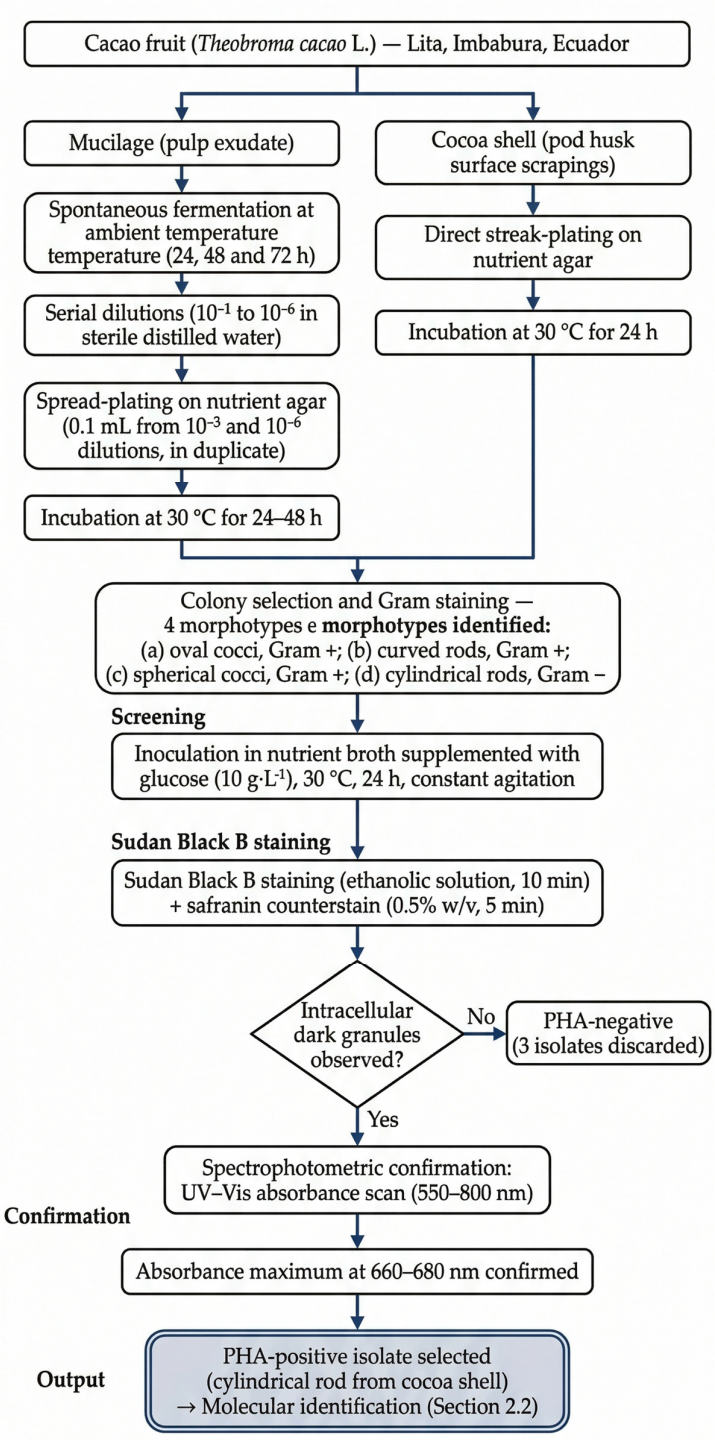

Figure 1. Schematic workflow for the isolation and screening of PHA-producing microorganisms from cocoa fruit residues.

For the cacao shell fraction, the outer surface of the pod husk was not subjected to the washing and disinfection protocol to preserve the native microbial communities associated with the fruit surface. Scrapings from the shell surface were collected and inoculated directly onto nutrient agar plates using the streak plate method.

 doi:10.20944/preprints202603.2393.v1

2.1.2. Recovery and Preliminary Identification of Isolates

Nutrient agar (Dibico S.A., Mexico) was used as the general-purpose isolation medium for both sample types, as it supports the growth of a broad range of bacterial and fungal species [26]. For the mucilage-derived samples, 0.1 mL aliquots from the 10^{-3} and 10^{-6} dilutions corresponding to each fermentation time point were spread-plated in duplicate onto nutrient agar and incubated at 30 °C for 24–48 h. Shell scrapings were streak-plated onto nutrient agar and incubated at 30 °C for 24 h. Following incubation, morphologically distinct colonies were selected and subjected to Gram staining as an initial phenotypic characterisation step to determine cell morphology and Gram reaction [27].

2.1.3. Screening for PHA Accumulation by Sudan Black B Staining

Representative colonies from each morphological group were inoculated into 5 mL of nutrient broth supplemented with glucose at a concentration of 10 $g \cdot L^{-1}$ to provide an excess carbon source favouring PHA accumulation. Cultures were incubated at 30 °C under constant agitation for 24 h [28–30]. After incubation, bacterial smears were prepared on sterile glass slides, heat-fixed and stained with an ethanolic solution of Sudan Black B for 10 min. The slides were subsequently washed with running water, air-dried and counterstained with 0.5% (w/v) safranin for 5 min, followed by a final wash with water [31,32]. The presence of dark grey or black intracellular granules in pink-stained vegetative cells was interpreted as a positive result indicating PHA accumulation.

2.1.4. Spectrophotometric Confirmation of Intracellular PHA

The presence of intracellular PHA in the Sudan Black B-positive isolate was further confirmed using the spectrophotometric method described by Porras et al. [25]. Stained cell suspensions were subjected to absorbance scanning in a UV–Vis spectrophotometer over the wavelength range of 550–800 nm. In this assay, cells containing intracellular PHA granules stained with Sudan Black B exhibit a characteristic absorbance maximum in the region of 660–680 nm, which serves as a confirmatory criterion for polymer accumulation, whereas PHA-negative cells display a flat or monotonically decreasing spectral profile across the same range [25].

2.2. Molecular Identification of the PHA-Positive Strain

2.2.1. Genomic DNA Extraction and 16S rRNA Gene Amplification

The PHA-positive isolate recovered from the cocoa shell (designated strain NBP01-UTN) was subjected to molecular identification based on 16S rRNA gene sequencing. Genomic DNA was extracted from a pure culture grown overnight on nutrient agar at 30 °C using a commercial genomic DNA extraction kit, following the manufacturer's instructions. The quality and concentration of the extracted DNA were assessed by agarose gel electrophoresis and spectrophotometric measurement, respectively.

The 16S rRNA gene was amplified by polymerase chain reaction (PCR) using the universal bacterial primers 27F (5′-AGAGTTTGATCMTGGCTCAG-3′) and 1492R (5′-TACGGYTACCTTGTTACGACTT-3′) [33]. PCR amplification was performed in a total reaction volume of 25 µL containing 12.5 µL of 2× PCR Master Mix (comprising Taq DNA polymerase, dNTPs and MgCl2), 1.0 µL of each primer (10 µM), 2.0 µL of template DNA (~50 ng) and 8.5 µL of nuclease-free water. The thermal cycling programme consisted of an initial denaturation at 95 °C for 5 min, followed by 35 cycles of denaturation at 95 °C for 30 s, primer annealing at 55 °C for 30 s and extension at 72 °C for 90 s, with a final extension step at 72 °C for 10 min. The resulting amplicons were verified by electrophoresis on a 1.0% (w/v) agarose gel stained with ethidium bromide (0.5 $\mu g \cdot mL^{-1}$) and visualised under UV transillumination. A single band of the expected size (~1450 bp) confirmed successful amplification. The PCR product was subsequently purified using a commercial PCR clean-up kit before sequencing.

 doi:10.20944/preprints202603.2393.v1

2.2.2. Sequencing and Sequence Analysis

The purified amplicon was submitted to Macrogen Inc. (Seoul, Republic of Korea) for bidirectional Sanger dideoxy sequencing using the same primer pair employed for amplification. Forward and reverse chromatograms were inspected for quality, trimmed, and assembled into an 862 bp consensus sequence corresponding to a partial fragment of the 16S rRNA gene of strain NBP01-UTN. The consensus sequence was deposited in the GenBank database of the National Centre for Biotechnology Information (NCBI) under accession number OR567321.1.

The obtained nucleotide sequence was compared against the NCBI non-redundant nucleotide database using the Basic Local Alignment Search Tool (BLASTn) [34] to identify the closest phylogenetic relatives. The search was restricted to type-strain sequences in the 16S ribosomal RNA database (Bacteria and Archaea) to ensure taxonomically reliable identification.

2.2.3. Phylogenetic Analysis

Multiple sequence alignment of the 16S rRNA gene sequences was performed using the ClustalW algorithm [35] implemented in MEGA 11 [36]. A phylogenetic tree was constructed using the Neighbour-Joining method [37] with evolutionary distances computed according to the Kimura 2-parameter model [38]. The robustness of the inferred tree topology was evaluated by bootstrap analysis with 1000 replicates [39]. The analysis included 16S rRNA gene sequences of type strains from all recognised species within the genus *Priestia*, retrieved from the NCBI GenBank database: *P. aryabhattai* (NR 115953.1), *P. megaterium* (NR 043401.1), *P. flexa* (NR 024691.1), *P. veravalensis* (NR 178610.1), *P. paraflexa* (NR 135732.1), *P. qingshengii* (NR 133978.1), *P. abyssalis* (NR 109671.1), *P. koreensis* (NR 043084.1), *P. taiwanensis* (NR 136461.1), *P. endophytica* (NR 025122.1) and *P. filamentosa* (NR 134701.1).

It should be noted that the genus *Priestia* was established by Gupta et al. [40] following a comprehensive phylogenomic study that reclassified several former *Bacillus* species—including *B. megaterium* and *B. aryabhattai*—into the newly proposed genus based on two conserved signature indels (CSIs) in the oligoribonuclease NrnB uniquely shared by all members of the *Megaterium* clade. The taxonomic nomenclature employed throughout the present manuscript follows this updated classification.

2.3. Physicochemical Characterisation of Cocoa Mucilage

Before use as a fermentation substrate, the raw cocoa mucilage underwent physicochemical characterisation to determine its composition and suitability as a carbon source for PHA production. The following analyses were performed in triplicate, and results are expressed as the mean ± standard deviation.

2.3.1. Ash Content

The total ash content of the cocoa mucilage was determined gravimetrically following the AOAC general procedure [41]. Approximately 5–10 g of raw mucilage was weighed into a pre-tared porcelain crucible and placed in a muffle furnace at 550 °C for 4–6 h until complete carbonisation was achieved. After the furnace temperature had decreased to at least 250 °C, the crucible was carefully transferred to a desiccator containing porcelain plates and a desiccant agent and allowed to cool to ambient temperature. The residual mass was weighed, and the ash content was calculated as a percentage of the original sample mass.

2.3.2. pH Determination

The pH of the cocoa mucilage was measured according to the AOAC method 981.12 [41]. A 25 mL sample of filtered and homogenised mucilage was measured directly with a calibrated digital pH meter (Milwaukee pH55; Milwaukee Instruments, Rocky Mount, NC, USA). The instrument was calibrated before each measurement session with standard buffer solutions at pH 7.00 and pH 4.01.

 doi:10.20944/preprints202603.2393.v1

2.3.3. Reducing Sugars

The total reducing sugar content was quantified by the 3,5-dinitrosalicylic acid (DNS) colourimetric method [42]. A calibration curve was first constructed using glucose standards at concentrations ranging from 0 to 2 g·L⁻¹. For each determination, 0.5 mL of appropriately diluted mucilage sample was mixed with 0.5 mL of DNS reagent in a 10 mL test tube. The mixture was heated in a boiling water bath for 5 min, rapidly cooled to ambient temperature and homogenised by gentle agitation. Absorbance readings were taken at 540 nm using a UV–Vis spectrophotometer. The concentration of reducing sugars was calculated from the linear regression equation of the calibration curve, applying a dilution factor of 500, and expressed as a percentage (m/v).

2.3.4. Free Glucose

Free glucose was determined by the glucose oxidase–peroxidase (GOD-PAP) enzymatic colourimetric method [43]. The assay is based on the oxidation of glucose by glucose oxidase, generating hydrogen peroxide, which subsequently reacts with 4-aminoantipyrine and phenol in the presence of peroxidase to form a red quinoneimine dye. The colour intensity is directly proportional to the glucose concentration in the sample. For each assay, 20 µL of mucilage sample (or glucose standard) was mixed with 2 mL of GOD-PAP working reagent. The mixture was incubated at ambient temperature for 10 min, and the absorbance was measured at 500 nm using a UV–Vis spectrophotometer against a reagent blank. The glucose concentration was calculated according to Equation (1):

$$C^{sample} = (A^{sample}/A^{standard}) \times C^{standard} \quad (1)$$

where A^{sample} and $A^{standard}$ denote the absorbance of the sample and the glucose standard, respectively, and $C^{standard}$ is the concentration of the glucose standard (mg·dL⁻¹). Results were converted and expressed as a percentage (m/v).

2.3.5. Mucilage Preparation for Fermentation

Before its use as a fermentation substrate, the raw mucilage was filtered through a sterile cotton cloth supported on a glass funnel to remove large fibrous particles. The filtered mucilage was then diluted to 50% (v/v) with a mixture of sterile distilled water and 2 N NaOH (1:1), the latter being used to adjust the pH to the value required for each experimental treatment (see Section 2.4). This dilution step was necessary to reduce the carbon source concentration to approximately 24.84 ± 1.03 g·L⁻¹ of reducing sugars, which is below the inhibitory threshold of 30 g·L⁻¹ typically recommended for batch fermentation processes [44]. The diluted and pH-adjusted mucilage was sterilised by autoclaving at 121 °C for 15 min before inoculation.

2.4. Experimental Design and Optimisation of PHA Production

2.4.1. Response Surface Methodology and Central Composite Design

The optimisation of PHA production by *Priestia aryabhattai* strain NBP01-UTN grown on cocoa mucilage was carried out using Response Surface Methodology (RSM) with a Central Composite Design (CCD). Three independent variables were evaluated as factors: temperature (Factor A), pH (Factor B) and the concentration of ammonium sulphate [$(NH_4)_2SO_4$] as an external nitrogen source (Factor C). The experimental ranges for each factor were established based on preliminary screening experiments and relevant literature on PHA production by *Priestia* spp. [13,45]. The factor levels and coded values are summarised in Table 1.

 doi:10.20944/preprints202603.2393.v1

Table 1. Independent variables and their experimental ranges in Central Composite Design.

Factor	Symbol	Unit	Low (-1)	Centre (0)	High (+1)
Temperature	A	°C	25.0	32.5	40.0
pH	B	–	6.5	7.5	8.5
$(NH_4)_2SO_4$ conc.	C	$g \cdot L^{-1}$	0.0	0.6	1.2

The CCD comprised a total of 20 experimental runs: 8 factorial points (23), 6 axial (α) points and 6 replications at the centre point. The axial distance was set at $\alpha = 1.6818$ (rotatable design), generating axial values of 19.9 °C and 45.1 °C for temperature, 5.82 and 9.18 for pH, and 0.0 and 1.61 $g \cdot L^{-1}$ for ammonium sulphate concentration. However, the axial low for Factor C should be 0.6 − (1.6818 × 0.6) = −0.409 g·L−1, which is physically impossible (negative concentration). This factor has truncated this to 0.0 $g \cdot L^{-1}$. The design matrix was generated, and the data were analysed using Python 3.11.x with the *statsmodels* and *SciPy* libraries. The response variable was the maximum PHA concentration ($g \cdot L^{-1}$) attained during each fermentation run. A second-order polynomial regression model was fitted to the experimental data, and its adequacy was evaluated by analysis of variance (ANOVA), including the determination of the coefficient of determination (R^2), adjusted R^2, lack-of-fit test and the F-test for overall model significance at a confidence level of 95% ($p < 0.05$).

2.4.2. Preparation for the Working Cell Bank

A working cell bank (WCB) was prepared to ensure uniform inoculum delivery across all experimental treatments. A pure culture of strain NBP01-UTN was inoculated into nutrient broth and incubated at 40 °C for 12 h to maximise biomass accumulation. The resulting culture was centrifuged at 4000 rpm for 20 min; the supernatant was discarded, and the pelleted biomass was resuspended in 20 mL of freshly prepared nutrient broth. The cell suspension was homogenised and distributed into 20 cryovials, each supplemented with 1 mL of 80% (v/v) glycerol as a cryoprotectant. The vials were stored at −4 °C until use. The elevated glycerol concentration (compared to the conventional 15–30%) was necessary to maintain cell viability under the slower freezing rate achievable with a standard laboratory freezer. The initial cell concentration in the inoculum was determined to be 0.0104 $g \cdot mL^{-1}$.

2.4.3. Submerged Fermentation Conditions

Submerged fermentation was conducted in a stirred-tank bioreactor operated in batch mode, with a total vessel capacity of 1.14 L and a working volume of 0.91 L (80% of the total). The bioreactor was equipped with an automatic controller for pH and temperature, and a magnetic stirring motor for continuous agitation. For each experimental run, the sterilised cocoa mucilage substrate (prepared as described in Section 2.3.5) was supplemented with the appropriate quantity of $(NH_4)_2SO_4$ as specified by the CCD, and the pH was adjusted to the target value with 2 N NaOH prior to autoclaving (121 °C, 15 min). One cryovial from the WCB was thawed and inoculated into a sterile substrate for each treatment.

Fermentation progress was monitored by withdrawing 50 mL samples at 4 h intervals over a total period of 32 h. The maximum PHA concentration recorded over the time course of each run was used as the response value for statistical analysis.

2.4.4. PHA Recovery and Gravimetric Quantification

PHA was recovered from the fermentation broth using a three-stage extraction protocol adapted from Abid et al. [46]. In the first stage (cell harvesting), 50 mL culture samples were centrifuged at 3000 rpm for 30 min. The resulting cell pellet was washed three times with sterile distilled water to remove residual medium components. In the second stage (cell disruption), the washed pellet was treated with 5% (v/v) sodium hypochlorite for 2 h to induce cell lysis and liberate the intracellular PHA granules. In the third stage (polymer solubilisation and recovery), 1 mL of chloroform was

 doi:10.20944/preprints202603.2393.v1

added to the disrupted cell suspension, mixed thoroughly with a micropipette and left to stand for 20 min to solubilise the polymer. The mixture was then centrifuged at 3000 rpm for 5 min, yielding a clear phase separation between the chloroform–PHA solution and the residual cell debris. The chloroform phase was carefully withdrawn using a micropipette and transferred to pre-weighed glass vials. The solvent was evaporated at 45 °C using a laboratory evaporator, and the dry polymer mass was recorded. The PHA concentration ($g \cdot L^{-1}$) was calculated from the recovered dry mass relative to the original sample volume.

2.4.5. Statistical Analysis

The experimental results were analysed using Python 3.11.x with the *statsmodels* and *SciPy* libraries. The significance of the overall model, individual linear terms, interaction terms and quadratic terms was assessed by ANOVA. The optimal fermentation conditions for maximum PHA production were determined using the software's numerical optimisation function (desirability approach). Validation runs were subsequently performed under the predicted optimal conditions to confirm the model predictions.

2.5. PHA Extraction and Characterisation

The PHA recovered under the optimised fermentation conditions (see Section 2.4) was subjected to structural and thermal characterisation to confirm its identity and assess its physicochemical properties.

2.5.1. Fourier-Transform Infrared Spectroscopy (FTIR)

The functional group composition of the extracted polymer was analysed by Fourier-transform infrared spectroscopy (FTIR) using an Agilent Technologies MicroLab FTIR spectrometer (Agilent Technologies, Santa Clara, CA, USA) equipped with a diamond attenuated total reflectance (ATR) accessory. Spectra were recorded in transmittance mode over the mid-infrared range of 4000–400 cm^{-1} at a spectral resolution of 4 cm^{-1}. Each spectrum was obtained as the average of 8 sample scans against a background of 8 scans, employing Happ–Genzel apodisation. A small quantity of the dried PHA film recovered after chloroform evaporation (Section 2.4.4) was placed directly on the ATR crystal for measurement. Three independent polymer samples (designated M1A, M2B and M2B2) were analysed to assess reproducibility. The recorded spectra were compared with characteristic absorption bands reported in the literature for poly(3-hydroxybutyrate) (PHB) and related polyhydroxyalkanoates [47,48].

2.5.2. Differential Thermal Analysis (DTA)

The thermal behaviour of the produced PHA was evaluated by differential thermal analysis (DTA) using a Mettler Toledo STARe system (Mettler Toledo, Columbus, OH, USA). Approximately 3.5 mg of dried polymer sample was weighed into a sealed aluminium pan. An empty sealed pan was used as the reference. The analysis was carried out under a nitrogen atmosphere over a temperature range of 15 to 250 °C using a two-step heating programme at a heating rate of 10 $°C \cdot min^{-1}$. The heat flow signal was recorded with the endothermic direction pointing upward (Endo Up convention). The resulting thermogram was analysed to identify thermal transitions, including the glass transition temperature (Tg), cold crystallisation events and the melting temperature (Tm). The onset, peak and end temperatures, as well as the enthalpy of fusion (ΔHm), were determined from the endothermic peaks using the instrument's integrated STARe software [49].

The thermal parameters obtained were compared with literature values for standard PHB and PHA copolymers to support identification of the polymer type and to evaluate its crystallinity and thermal stability, which are key factors that determine the processability and potential applications of the bioplastic [50,51].

 doi:10.20944/preprints202603.2393.v1

2.6. Statistical Analysis

All physicochemical determinations of the cocoa mucilage (ash content, pH, reducing sugars and free glucose) were performed in triplicate, and the results are reported as the arithmetic mean ± standard deviation (SD). The spectrophotometric confirmation of intracellular PHA using the Sudan Black B method was likewise performed in triplicate for the positive isolate.

The experimental data from the Central Composite Design (CCD) were analysed using Python 3.11.x with the *statsmodels* and *SciPy* libraries. The complete analysis script is provided as Supplementary Material S1. A second-order polynomial regression model (Equation (2)) was fitted to the response variable (maximum PHA concentration, g·L^{-1}):

$$Y = \beta_0 + \sum \beta_i X_i + \sum \beta_{ii} {X_i}^2 + \sum \beta_{ij} X_i X_j \quad (2)$$

where Y is the predicted response; β_0 is the intercept coefficient; β_i, β_{ii} and β_{ij} are the linear, quadratic and interaction regression coefficients, respectively; X_i and X_j represents the coded independent variables ($i \neq j$); and ε is the random error term.

The statistical significance of the overall model, as well as the individual linear, quadratic and interaction terms, was assessed by analysis of variance (ANOVA). The adequacy of the fitted model was evaluated on the basis of the following criteria: the Fisher's F-test and associated *p*-value for overall model significance (at a confidence level of 95%, $\alpha = 0.05$); the coefficient of determination (R^2) and adjusted R^2 (R^2_{adj}) to assess the proportion of variance explained by the model; the predicted R^2 (R^2_{pred}) to evaluate the model's predictive capability; the lack-of-fit test to verify that the model adequately described the experimental data; and the coefficient of variation (C.V.%) as a measure of reproducibility. A difference of less than 0.2 between R^2_{adj} and R^2_{pred} was considered indicative of reasonable agreement between the two metrics [52].

The optimal fermentation conditions for maximising PHA production were identified using the numerical optimisation function implemented in Python 3.11.x [53]. Three-dimensional response surface plots and contour plots were generated to visualise the effects of the pairwise interactions between factors on the response variable. Validation experiments were subsequently conducted under the predicted optimal conditions to confirm the accuracy of the model predictions.

Throughout the study, differences were considered statistically significant at $p < 0.05$ unless otherwise stated.

3. Results and Discussion

3.1. Isolation and Selection of PHA-Producing Bacteria

3.1.1. Morphological Diversity of Isolates from Cocoa Fruit Residues

A total of four morphologically distinct microbial types were recovered from the two cocoa fruit fractions examined. Three morphotypes were isolated from the mucilage samples during the spontaneous fermentation at ambient temperature (24–48 h), whilst a fourth morphotype was recovered exclusively from the surface of the cocoa pod shell. The preliminary phenotypic characterisation of each isolate by Gram staining is summarised in Table 2.

Table 2. Morphological and phenotypic characterisation of microbial isolates recovered from cocoa fruit residues.

Isolate	Source	Cell morphology	Gram reaction	Presumptive identity	Sudan Black B
(a)	Mucilage (24 h)	Oval cocci	Positive	*Hanseniaspora* spp.	Negative
(b)	Mucilage (24-48 h)	Curved rods	Positive	*Lactobacillus* spp.	Negative
(c)	Mucilage (48 h)	Spherical cocci	Positive	*Lactobacillus* spp.	Negative
(d)	Cocoa shell	Cylindrical rods	Negative [1]	*Bacillus*-like	Positive

[1] See discussion below regarding Gram-variable reaction in *Priestia* spp.

 doi:10.20944/preprints202603.2393.v1

The three mucilage-derived morphotypes (a–c) correspond to the well-characterised microbial succession that occurs during the natural fermentation of cocoa pulp [54,55]. Morphotype (a), comprising oval Gram-positive cocci isolated during the first 24 h of fermentation, was consistent with the yeast genus *Hanseniaspora*, which dominates the early fermentative phase owing to its tolerance of the high sugar content and low pH of fresh mucilage [54]. Morphotype (b), identified as Gram-positive curved rods recovered between 24 and 48 h, was consistent with lactic acid bacteria (*Lactobacillus* spp.), which proliferate following the rapid consumption of dissolved oxygen by yeasts, thereby creating microaerobic conditions favourable to this group [55]. Morphotype (c), spherical Gram-positive cocci appearing at approximately 48 h, was attributed to acetic acid bacteria, whose emergence is driven by the pectinolytic degradation of the mucilaginous tissue and the concomitant increase in aeration and consumption of citric acid [54,55].

In contrast, morphotype (d)—large cylindrical rods isolated from the cocoa shell surface—did not correspond to the typical cocoa fermentation microbiota. Based on its morphology and colony characteristics (rod-shaped, endospore-forming, growth at elevated temperatures of up to 45 °C and preference for neutral pH), this isolate was provisionally assigned to the genus *Bacillus* sensu lato. Subsequent molecular identification (Section 3.2) confirmed the isolate as *Priestia aryabhattai* strain NBP01-UTN. Notably, the Gram staining reaction of this isolate was negative under the conditions employed, although *P. aryabhattai* is taxonomically classified as a Gram-positive organism [18]. This apparent discrepancy is consistent with the well-documented phenomenon of Gram-variable behaviour in members of the *Priestia* (formerly *Bacillus*) clade, which may yield Gram-negative results depending on the growth phase, culture age and physiological state at the time of staining [19,56].

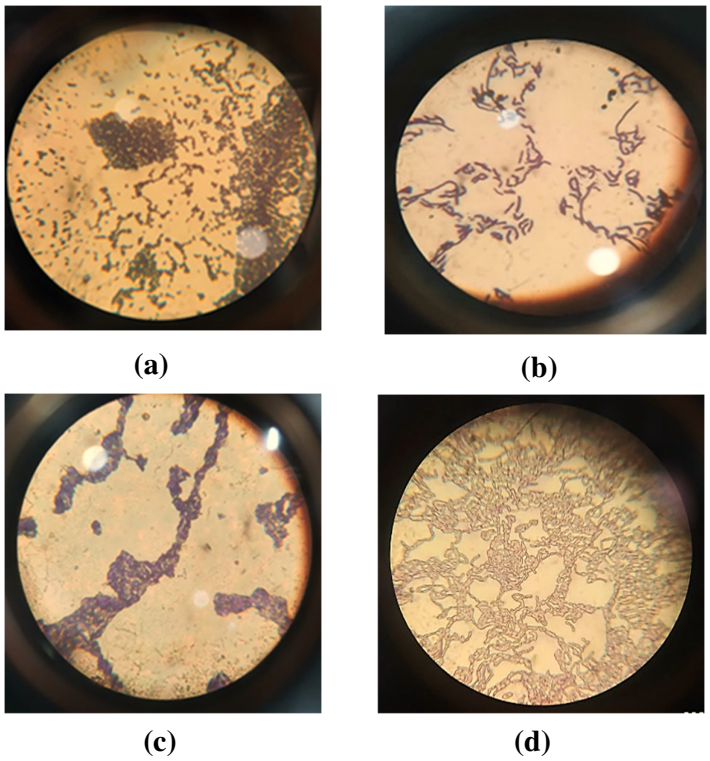

Figure 2. Light micrographs of Gram-stained microbial isolates recovered from cocoa fruit residues: (a) oval cocci from mucilage (24 h, Gram-positive); (b) curved rods from mucilage (24–48 h, Gram-positive); (c) spherical cocci from mucilage (48 h, Gram-positive); (d) cylindrical rods from cocoa shell (Gram-negative reaction).

3.1.2. Screening for PHA Accumulation by Sudan Black B Staining

All four isolates were screened for intracellular PHA accumulation using Sudan Black B staining after cultivation in glucose-supplemented nutrient broth (10 g·L^{-1} glucose, 30 °C, 24 h). Of the four

 doi:10.20944/preprints202603.2393.v1

morphotypes evaluated, only isolate (d)—the cylindrical rod recovered from the cocoa shell—exhibited a positive Sudan Black B reaction, characterised by the presence of dark grey to black intracellular granules clearly discernible within the pink safranin-counterstained vegetative cells (Table 2; Figure 3d). The three mucilage-derived isolates (a–c) displayed uniformly pink cells without detectable intracellular granules, indicating the absence of PHA accumulation under the conditions tested (Figure 3a–c).

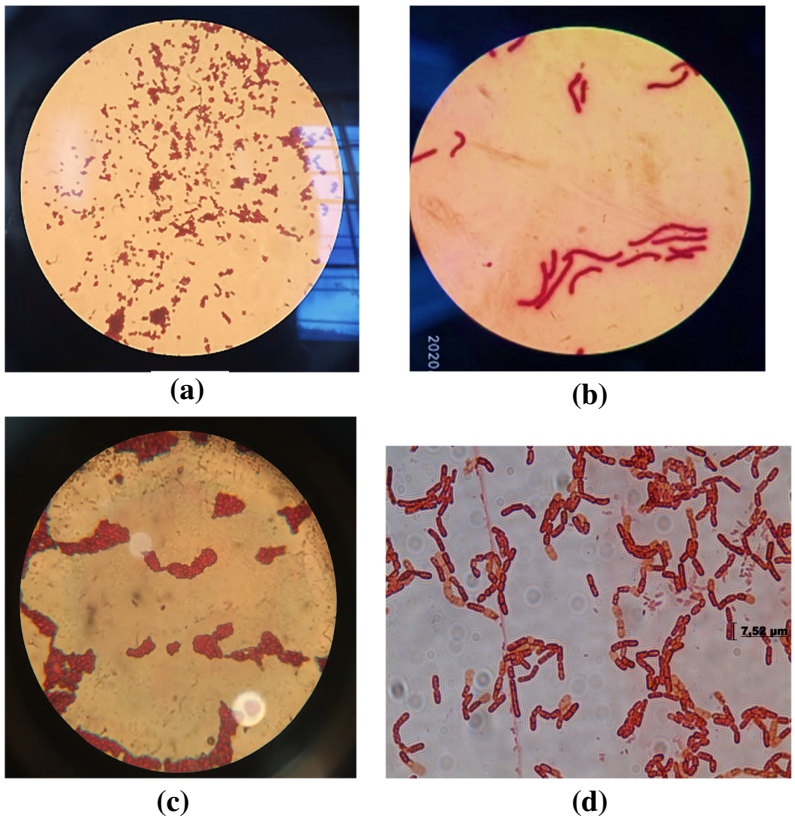

Figure 3. Sudan Black B staining micrographs of microbial isolates from cocoa fruit residues: (a) oval cocci, PHA-negative; (b) curved rods, PHA-negative; (c) spherical cocci, PHA-negative; (d) cylindrical rods from cocoa shell, PHA-positive, showing dark intracellular granules (arrows) within safranin-counterstained vegetative cells. The isolate shown in (d) was subsequently identified as *Priestia aryabhattai* strain NBP01-UTN by 16S rRNA gene sequencing.

The finding that only one out of four isolates tested positive for PHA accumulation is consistent with the general observation that, whilst numerous bacterial species can synthesise PHAs, only a fraction of the cultivable microbiota in any given environmental niche possesses this metabolic capacity [57,58]. In a comparable screening study, Muneer et al. [7] reported that approximately 25–35% of bacterial isolates from diverse environmental sources tested positive for PHA by Sudan Black B staining. Similarly, Sachan et al. [59] recently identified *Bacillus megaterium* MTCC 453 as a PHA producer from wheat straw waste using the same staining protocol. The isolation of the PHA-positive strain exclusively from the cocoa shell—rather than from the mucilage—is noteworthy, as it suggests that the surface microbiota of the cacao pod may harbour PHA-producing endospore-forming bacteria associated with the soil and phyllosphere environment, distinct from the fermentative microbiota of the mucilage.

 doi:10.20944/preprints202603.2393.v1

3.1.3. Spectrophotometric Confirmation of Intracellular PHA

The intracellular accumulation of PHA in isolate (d) was further validated using the Sudan Black B spectrophotometric method described by Porras et al. [25]. The UV–Vis absorbance spectra of Sudan Black B-stained cell suspensions of the PHA-positive isolate ('Cepa' 1.2.1) and a representative PHA-negative isolate ('Cepa' 2.2) are presented in Table 3 and Figure 4.

Table 3. UV–Vis absorbance values (550–800 nm) for the PHA-positive isolate ('Cepa' 1.2.1; mean ± SD, n = 3) and the PHA-negative isolate ('Cepa' 2.2) after Sudan Black B staining.

Wavelength (nm)	'Cepa' 1.2.1 (PHA+) Abs.	'Cepa' 2.2 (PHA -) Abs.
550	0.641 ± 0.008	0.235
600	0.719 ± 0.012	0.258
630	0.757 ± 0.015	0.264
650	0.782 ± 0.007	0.268
660	0.787 ± 0.007	0.275
665	**0.788 ± 0.004**	–
670	0.775 ± 0.007	0.265
680	0.751 ± 0.009	0.261
700	0.718 ± 0.003	0.250
750	0.609 ± 0.003	0.222
800	0.529 ± 0.004	0.195

Bold values indicate the absorbance maximum region (660–665 nm) diagnostic for PHA. SD: standard deviation. Abs.: absorbance.

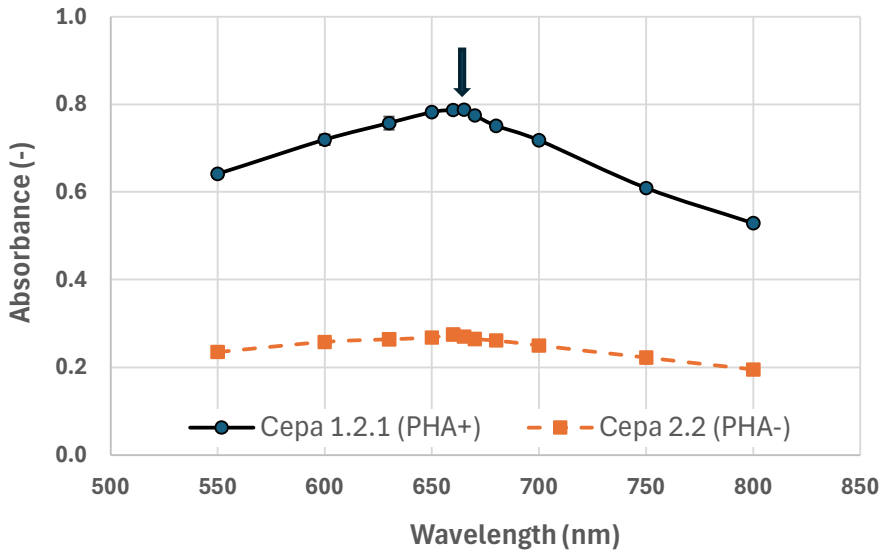

Figure 4. UV–Vis absorbance spectra (550–800 nm) of Sudan Black B-stained cell suspensions: PHA-positive isolate Cepa 1.2.1 (solid black line, mean ± SD, n = 3) and PHA-negative isolate Cepa 2.2 (orange dashed line). The arrow indicates the absorbance maximum at 665 nm, which is diagnostic of intracellular PHA granules.

The PHA-positive isolate exhibited a characteristic spectral profile with a well-defined absorbance maximum at 665 nm (mean absorbance = 0.788 ± 0.004), with elevated values sustained across the 660–680 nm region (Table 3). This spectral signature is consistent with the criterion established by Porras et al. [25], who demonstrated that Sudan Black B-stained cells containing intracellular PHA granules exhibit absorbance maxima between 660 and 680 nm, attributable to the

 doi:10.20944/preprints202603.2393.v1

lipophilic dye's selective affinity for the hydrophobic polyester inclusions. In contrast, the PHA-negative isolate ('Cepa' 2.2) displayed a markedly flatter, lower-absorbance profile across the entire scanned range (maximum absorbance of 0.275 at 660 nm), with no discernible peak in the diagnostic region, confirming the absence of intracellular polymer.

The approximately threefold difference in absorbance at 665 nm between the PHA-positive (0.788) and PHA-negative (estimated ~0.270) isolates provides a clear quantitative distinction that reinforces the qualitative Sudan Black B microscopic observation. The high reproducibility of the spectral measurements across the three replicates of the PHA-positive strain (coefficients of variation < 2% at the peak wavelength) further supports the reliability of this method for rapid screening. These spectrophotometric results, together with the microscopic evidence, unequivocally confirmed that isolate (d) from the cocoa shell accumulated intracellular PHA granules and was therefore selected for molecular identification (Section 3.2) and subsequent use as the production strain in the fermentation optimisation studies (Section 3.4).

The combination of Sudan Black B microscopy with spectrophotometric confirmation represents a practical two-tier screening approach that can be readily implemented in resource-limited laboratory settings. This is particularly relevant to the present study, which was conducted under the operational constraints imposed by the COVID-19 pandemic. More specific fluorescence-based staining methods (e.g., Nile Red A or Nile Blue A) offer greater sensitivity and can differentiate between PHA types [57,60]. Whilst the Sudan Black B-based protocol employed here was sufficient to identify and select a PHA-producing strain from cocoa fruit residues.

3.2. Molecular Identification

The partial 16S rRNA gene sequence of isolate (d), designated strain NBP01-UTN, was determined by bidirectional Sanger sequencing and assembled into an 862 bp consensus contig. The sequence was deposited in the GenBank database of the National Centre for Biotechnology Information (NCBI) under accession number OR567321.1. Comparison of the 862 bp sequence against the NCBI 16S ribosomal RNA database (Bacteria and Archaea) restricted to type-strain entries using the BLASTn algorithm [34] yielded *Priestia aryabhattai* type strain B8W22T (accession NR_115953.1) as the closest match, with 99.88% sequence identity and 100% query coverage (E-value = 0.0). The second-highest scoring hit corresponded to *Priestia megaterium* type strain NBRC 15308T (NR_043401.1), with a marginally lower identity of 99.52% and a query coverage of 97% (E-value = 0.0). These values are well above the 98.65% threshold currently recommended for species-level delineation based on 16S rRNA gene sequences [61], thereby supporting the assignment of strain NBP01-UTN to the species *P. aryabhattai*.

The phylogenetic relationships of strain NBP01-UTN were further evaluated by constructing a Neighbour-Joining tree [37] using partial 16S rRNA gene sequences from type strains representing all eleven currently recognised species within the genus *Priestia* [18]. Evolutionary distances were computed using the Kimura 2-parameter model [38], and branching robustness was assessed by bootstrap analysis with 1000 replicates [39] (Figure 5).

 doi:10.20944/preprints202603.2393.v1

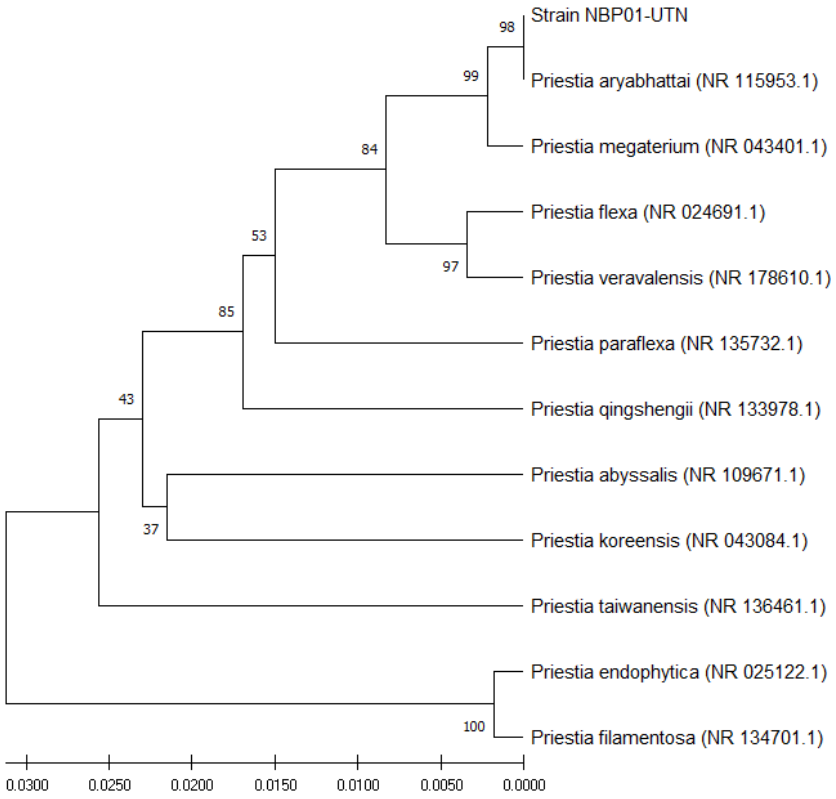

Figure 5. Neighbour-Joining phylogenetic tree based on partial 16S rRNA gene sequences showing the relationship of strain NBP01-UTN to type strains of all recognised *Priestia* species. Evolutionary distances were computed using the Kimura 2-parameter model [38]. Numbers at nodes indicate bootstrap support values (%) from 1000 replicates [39]; only values ≥38% are shown. GenBank accession numbers for each type strain are indicated in parentheses. The scale bar represents the number of base substitutions per site.

In the resulting dendrogram, strain NBP01-UTN clustered tightly with the type strain of *P. aryabhattai* (NR_115953.1), forming a well-supported terminal clade with a bootstrap value of 97%. This *P. aryabhattai* clade was, in turn, grouped with *P. megaterium* (NR_043401.1) with strong support (99% bootstrap), consistent with the close phylogenetic affinity between these two sister species, whose 16S rRNA gene sequences share approximately 99.7% nucleotide identity [62]. The broader topology of the tree was congruent with recently published phylogenies of the genus [18,63], with *P. flexa* and *P. veravalensis* forming a well-supported subclade (96% bootstrap support), and the more distantly related *P. endophytica* and *P. filamentosa* forming a distinct outgroup pair (100% bootstrap support).

The high sequence similarity between *P. aryabhattai* and *P. megaterium* (>99%) has been the subject of considerable taxonomic debate. Although *P. aryabhattai* was originally described as a novel species of the genus Bacillus on the basis of low DNA–DNA hybridisation values and phenotypic distinctions [62] a subsequent proposal recommended its reclassification as a later heterotypic synonym of *P. megaterium*, as the average nucleotide identity (ANI) between their type-strain genomes exceeded the 95% species boundary [64]. However, the comprehensive phylogenomic study by Gupta et al. [18] transferred both taxa into the newly established genus *Priestia*, retaining them as distinct species based on conserved signature indels (CSIs) and whole-genome analyses. A very

 doi:10.20944/preprints202603.2393.v1

recent comparative genomic investigation has further supported their preservation as separate species, demonstrating that *P. aryabhattai* and *P. megaterium* form two congruent clades in core-genome phylogenies, notwithstanding limited evidence of inter-clade recombination [63]. In the present study, the preferential clustering of strain NBP01-UTN with *P. aryabhattai* rather than *P. megaterium*—supported by both BLASTn identity ranking and phylogenetic positioning—justifies its identification as *Priestia aryabhattai* strain NBP01-UTN.

This molecular identification also resolves the apparent discrepancy observed during the preliminary phenotypic characterisation of isolate (d), which displayed a Gram-negative reaction despite *P. aryabhattai* being classified as a Gram-positive organism (Table 2; Section 3.1.1). As discussed earlier, Gram-variable behaviour is well documented in the *Priestia* (formerly *Bacillus*) clade, with staining outcome influenced by growth phase, culture age and physiological state at the time of fixation [19,56]. The isolation of P. aryabhattai from the surface of the cocoa pod husk is ecologically coherent, as this species is widely distributed in soil, rhizosphere and phyllosphere environments [65] and has been reported as an endospore-forming, stress-tolerant bacterium capable of surviving on plant surfaces exposed to UV radiation and desiccation [62]. To the best of the authors' knowledge, the present study constitutes the first report of a PHA-producing *P. aryabhattai* strain isolated from cocoa (*Theobroma cacao* L.) fruit residues.

The capacity of *P. aryabhattai* to accumulate polyhydroxyalkanoates has been documented in a limited number of previous studies. Balakrishna Pillai et al. [60] reported short-chain-length PHA accumulation in *B. aryabhattai* (as it was then designated) using refined carbon sources under controlled laboratory conditions. More recently, Rysbek et al. [21] evaluated poly(3-hydroxybutyrate) production by *B. aryabhattai* RAF 5 using a periodic medium renewal strategy. The present strain, NBP01-UTN, therefore extends the range of known PHA-producing *P. aryabhattai* isolates and is, to the authors' knowledge, the first to be cultivated on a cocoa-derived substrate for bioplastic production, as described in Section 3.4.

3.3. Cocoa Mucilage Characterisation and Preparation

The physicochemical composition of the raw cocoa mucilage was determined prior to its use as a fermentation substrate, with the aim of confirming its suitability as a carbon source for PHA biosynthesis. The results of the four analytical determinations performed in triplicate are summarised in Table 4, together with literature reference ranges reported for Ecuadorian cocoa mucilage.

Table 4. Physicochemical characterisation of raw cocoa mucilage (*Theobroma cacao* L.). Values are expressed as the mean ± standard deviation (n = 3). Reference ranges are included for comparison.

Parameter	Result	Reference Range	References
Ash content (% (m/v))	0.39 ± 0.02	0.40–0.50	[66]
pH (—)	3.70 ± 0.05	3.30–4.00	[67]
Reducing sugars (% (m/v))	12.20 ± 0.72	12.50–15.90	[68]
Free glucose (% (m/v))	4.97 ± 0.21	4.81–6.91	[68]

The ash content of the mucilage was 0.39 ± 0.02% (m/v), which falls slightly below the range of 0.40–0.50% reported by Ortiz and Álvarez [66] for Ecuadorian cocoa mucilage. This minor difference of approximately 0.01% may be attributed to variations in the soil's mineral composition at the sites where the cacao trees were cultivated. The ash fraction is of practical interest because it contains inorganic salts—primarily oxides, sulphates, phosphates, and chlorides—that may serve as supplementary mineral nutrients for bacterial growth during fermentation [69,70].

The pH of the raw mucilage was measured at 3.70 ± 0.05, which falls within the typical range of 3.30–4.00 reported for cocoa mucilage by Wacher Rodarte [67]. This characteristically low pH results from the high content of citric acid naturally present in the pulp tissue [16]. Although the acidic environment of the raw mucilage favours the growth of yeasts and lactic acid bacteria during the spontaneous fermentation of cacao beans (as observed in Section 3.1), it is well below the optimal pH

 doi:10.20944/preprints202603.2393.v1

range of 6.0–8.5 required for the growth of most bacterial species, including members of the genus *Priestia* [71]. Consequently, pH adjustment with 2 N NaOH was necessary prior to fermentation, as described in Section 2.3.5. Importantly, this alkaline adjustment did not appreciably alter the concentration of the predominant carbon source (glucose), thereby preserving the substrate's nutritive value.

The total reducing sugar content was determined to be 12.20 ± 0.72% (m/v), corresponding to approximately 122 g·L^{-1} in the raw mucilage. This value is slightly below the range of 12.50–15.90% reported by Zambrano [68] for the same Ecuadorian cacao variety, although it remains within a comparable order of magnitude. The high sugar content confirms that cocoa mucilage is a carbohydrate-rich substrate with substantial potential for microbial fermentation that relies on reducing sugars as the primary carbon and energy source.

The free glucose concentration was 4.97 ± 0.21% (m/v), which falls within the range of 4.81–6.91% determined by Zambrano [68] for Ecuadorian cocoa mucilage. Glucose is one of the most readily assimilable carbon sources for a wide variety of heterotrophic bacteria, including PHA-producing strains of the genus *Priestia* [19]. However, the total carbon source concentration in the raw mucilage (approximately 49.7 g·L^{-1} free glucose) substantially exceeds the inhibitory threshold of 30 g·L^{-1}, which is generally recommended for batch fermentation processes to avoid substrate inhibition [44]. It was therefore essential to dilute the mucilage before its use as a fermentation substrate.

Following the dilution protocol described in Section 2.3.5, the cocoa mucilage was mixed 1:1 (v/v) with sterile distilled water, reducing the total reducing sugar concentration to approximately 24.84 ± 1.03 g·L^{-1}, a value safely below the 30 g·L^{-1} inhibitory ceiling [44]. The pH of the diluted mucilage was subsequently adjusted to the target value specified by each experimental treatment in the CCD (Section 2.4) using 2 N NaOH, and the prepared substrate was sterilised by autoclaving at 121 °C for 15 min. This two-step preparation strategy—dilution followed by pH adjustment—ensured that the fermentation medium provided an adequate but non-inhibitory concentration of fermentable carbon whilst simultaneously achieving neutral-to-mildly alkaline conditions that favour growth and PHA accumulation by the *P. aryabhattai* strain NBP01-UTN.

Taken together, the physicochemical data indicate that cocoa mucilage from Ecuadorian cacao possesses favourable compositional attributes for its valorisation as a low-cost fermentation feedstock. Its high reducing sugar content, combined with the presence of trace minerals in the ash fraction, makes it a suitable candidate for PHA production following minimal pre-treatment. These findings align with the broader strategy of converting agro-industrial waste streams into value-added bioproducts within a circular bioeconomy framework [12,16].

3.4. Optimisation of Fermentation Conditions for PHA Production

3.4.1. Central Composite Design: Experimental Results

A rotatable central composite design (CCD) comprising 20 experimental runs—eight factorial points, six axial points ($\alpha \approx 1.682$) and six centre-point replicates—was employed to investigate the combined effects of temperature (Factor A, 19.9–45.1 °C), pH (Factor B, 5.82–9.18) and ammonium sulphate concentration (Factor C, 0–1.61 g·L^{-1}) on PHA production by *Priestia aryabhattai* strain NBP01-UTN cultivated on diluted cocoa mucilage. The experimental matrix, together with the observed PHA concentrations recorded at 24 h of fermentation, is presented in Table 5.

Table 5. Central composite design matrix with coded and actual factor levels and observed PHA concentrations at 24 h of fermentation.

Std	Run	Type	Temperature (°C)	pH (–)	$(NH_4)_2SO_4$ (g·L^{-1})	PHA conc. (g·L^{-1})
1	7	Factorial	25.00	6.50	0.00	0.347
2	16	Factorial	40.00	6.50	0.00	0.496
3	9	Factorial	25.00	8.50	0.00	0.398

 doi:10.20944/preprints202603.2393.v1

4	15	Factorial	40.00	8.50	0.00	0.468
5	4	Factorial	25.00	6.50	1.20	0.267
6	13	Factorial	40.00	6.50	1.20	0.412
7	14	Factorial	25.00	8.50	1.20	0.288
8	8	Factorial	40.00	8.50	1.20	0.407
9	20	Axial	19.89	7.50	0.60	0.211
10	18	Axial	45.11	7.50	0.60	0.476
11	19	Axial	32.50	5.82	0.60	0.298
12	3	Axial	32.50	9.18	0.60	0.307
13	17	Axial	32.50	7.50	0.00	0.460
14	2	Axial	32.50	7.50	1.61	0.412
15	5	Centre	32.50	7.50	0.60	0.365
16	1	Centre	32.50	7.50	0.60	0.368
17	6	Centre	32.50	7.50	0.60	0.345
18	11	Centre	32.50	7.50	0.60	0.372
19	12	Centre	32.50	7.50	0.60	0.369
20	10	Centre	32.50	7.50	0.60	0.372

The observed PHA concentrations across the 20 experimental runs ranged from 0.211 to 0.496 g·L^{-1}, demonstrating that the selected factor ranges encompassed conditions of both markedly low and relatively high productivity. The highest PHA concentration (0.496 g·L^{-1}) was obtained under run 2 (standard order 2: 40 °C, pH 6.5, 0 g·L^{-1} ammonium sulphate), whereas the lowest value (0.211 g·L^{-1}) was recorded under run 9 (standard order 9: 19.9 °C, pH 7.5, 0.6 g·L^{-1} ammonium sulphate). This nearly 2.4-fold variation in PHA yield underscores the pronounced sensitivity of PHA biosynthesis in this strain to the fermentation parameters under investigation.

The six centre-point replicates (runs 15–20) yielded PHA concentrations ranging from 0.345 to 0.372 g·L^{-1}, with a mean of 0.365 ± 0.010 g·L^{-1}. The low standard deviation observed across these replicates confirms the satisfactory reproducibility of the fermentation process and supports the reliability of the experimental data for model fitting.

A preliminary inspection of the data reveals a clear trend wherein higher temperatures favoured PHA accumulation. Factorial runs conducted at 40 °C (runs 2, 4, 6 and 8) consistently produced higher PHA concentrations (0.407–0.496 g·L^{-1}) than their counterparts at 25 °C (runs 1, 3, 5 and 7; 0.267–0.398 g·L^{-1}). This observation is consistent with the known thermotolerant character of *Priestia* species, several of which have been reported to exhibit enhanced metabolic activity and PHA accumulation at temperatures above 30 °C [19,73]. The axial point at the highest temperature (45.1 °C, run 10) produced 0.476 g·L^{-1}, further supporting the positive influence of elevated temperature on PHA biosynthesis in this organism.

A second notable trend concerns the effect of the external nitrogen source. Within each pair of factorial runs differing only in ammonium sulphate concentration, the condition without nitrogen supplementation (0 g·L^{-1}) consistently outperformed the nitrogen-supplemented condition (1.2 g·L^{-1}). For example, run 2 (40 °C, pH 6.5, [$(NH_4)_2SO_4$] = 0) yielded 0.496 g·L^{-1} versus 0.412 g·L^{-1} for run 6 (40 °C, pH 6.5, [$(NH_4)_2SO_4$] = 1.2 g·L^{-1}). Similarly, the axial point without nitrogen (run 13: 0.460 g·L^{-1}) surpassed the high-nitrogen axial point (run 14: 0.412 g·L^{-1}). This pattern is physiologically consistent with the well-established principle that nitrogen limitation promotes the diversion of carbon flux towards PHA biosynthesis as a carbon and energy storage mechanism, rather than channelling it into protein synthesis and cell growth [74,75].

3.4.2. Regression Model and Analysis of Variance

The experimental data of response ($\hat{Y}_{PHA}$, g·L^{-1}) were fitted to a full second-order polynomial regression model using ordinary least squares (OLS) regression implemented in the *statsmodels* library for Python 3 [76]. The coded variables were defined as $A = (Temp - 32.5)/7.5$, $B = (pH - 7.5)/1.0$ and $C = (N - 0.6)/0.6$.

 doi:10.20944/preprints202603.2393.v1

The resulting regression equation in terms of the coded factors is:

$$\hat{Y}_{PHA} = 0.3655 + 0.0680 \cdot A + 0.0040 \cdot B - 0.0442 \cdot C - 0.0131 \cdot AB + 0.0056 \cdot AC - 0.0009 \cdot BC - 0.0067 \cdot A^2 - 0.0212 \cdot B^2 + 0.0455 \cdot C^2 \quad (3)$$

where $\hat{Y}_{PHA}$ denotes the predicted PHA concentration (g·L^{-1}). In terms of the actual (uncoded) factors, the equation becomes:

$$\hat{Y}_{PHA} = -1.5955 + 0.0291 \times Temp + 0.3797 \times pH - 0.2549 \times N - 0.00175 \times Temp \times pH + 0.00125 \times Temp \times N - 0.00146 \times pH \times N - 0.000118 \times Temp^2 - 0.0212 \times pH^2 + 0.1263 \times N^2 \quad (4)$$

The analysis of variance (ANOVA) for the fitted model is summarised in Table 6. The overall model was highly significant (F = 50.57, p < 0.0001), indicating that the selected factors exerted a meaningful influence on PHA production. Among the individual model terms, temperature (A) was the most influential variable (F = 283.58, p < 0.0001), followed by the nitrogen concentration (C; F = 93.33, p < 0.0001). The quadratic terms C² (F = 84.25, p < 0.0001) and B² (F = 29.22, p = 0.0003) were also highly significant, as was the temperature–pH interaction term AB (F = 6.19, p = 0.032). By contrast, pH as a linear term (B; p = 0.349) exerted a comparatively modest effect across the range tested, which may be attributable to the inherent buffering capacity of the cocoa mucilage substrate.

Table 6. Analysis of variance (ANOVA) for the quadratic regression model of PHA concentration.

Source	Sum of Squares	*df*	Mean Square	*F*-value	*p*-value	
Model	0.10136	9	0.01126	50.57	< 0.0001	***
A	0.06315	1	0.06315	283.58	< 0.0001	***
B	0.00021	1	0.00021	0.96	0.3493	
C	0.02078	1	0.02078	93.33	< 0.0001	***
AB	0.00138	1	0.00138	6.19	0.0321	*
AC	0.00025	1	0.00025	1.14	0.3114	
BC	0.00001	1	0.00001	0.03	0.8716	
A²	0.00064	1	0.00064	2.89	0.1197	
B²	0.00651	1	0.00651	29.22	0.0003	***
C²	0.01876	1	0.01876	84.25	< 0.0001	***
Residual	0.00223	10	0.00022			
Lack of Fit	0.00170	5	0.00034	3.26	0.1103	n.s.
Pure Error	0.00052	5	0.00010			
Cor Total	0.10359	19				

*** p < 0.001; * p < 0.05; n.s., not significant.

The fit statistics for the model are presented in Table 7. The coefficient of determination (R^2 = 0.9785) indicated that the model accounted for 97.85% of the variability in PHA concentration. The adjusted R^2 (R^2_{adj} = 0.9591) confirmed the model's adequacy after accounting for the number of predictors, and the predicted R^2 (R^2_{pred} = 0.8392) was in reasonable agreement with R^2_{adj} (difference = 0.12 < 0.2), supporting the model's predictive capability [77]. The adequate precision ratio of 17.80, well above the threshold of 4, indicated a satisfactory signal-to-noise ratio. The *coefficient of variation* (C.V. = 4.01%) further confirmed the high reproducibility of the experimental data. The lack-of-fit test was non-significant (F = 3.26, p = 0.110), confirming that the quadratic model adequately described the relationship between the factors and the response.

 doi:10.20944/preprints202603.2393.v1

Table 7. Fit statistics for the quadratic regression model.

Statistic	Value
R^2	0.9785
R^2 Adjusted	0.9591
R^2 Predicted	0.8392
Adequate Precision	17.80
C.V. %	4.01
Std. Dev.	0.0149
Mean	0.3719
PRESS	0.0166

3.4.3. Response Surface Analysis

Three-dimensional response surface plots and their corresponding two-dimensional contour plots were generated to visualise the interactive effects of the three factors on PHA production within the factorial region of the design (i.e., coded factor levels from −1 to +1, corresponding to 25–40 °C, pH 6.5–8.5 and 0–1.2 g·L^{-1} ammonium sulphate). Although the axial points ($\alpha \approx \pm 1.682$) extend beyond this region and were essential for reliable estimation of the quadratic coefficients, the response surface analysis was intentionally restricted to the factorial domain to ensure that all predicted optima lie within the region of highest model reliability [77].

Figure 6 illustrates the combined effect of temperature and pH on PHA concentration at a fixed nitrogen concentration of 0 g·L^{-1} (corresponding to the predicted optimum). The surface exhibits a clear ascending gradient as temperature increases from 25 to 40 °C, with a broad maximum in the neutral pH region (approximately pH 7.0–7.5). The elliptical contour lines indicate a moderate interaction between temperature and pH, consistent with the significant AB interaction term identified in the ANOVA ($p = 0.032$). The positive effect of temperature is the dominant feature of this surface, reflecting the thermotolerant nature of *P. aryabhattai* NBP01-UTN.

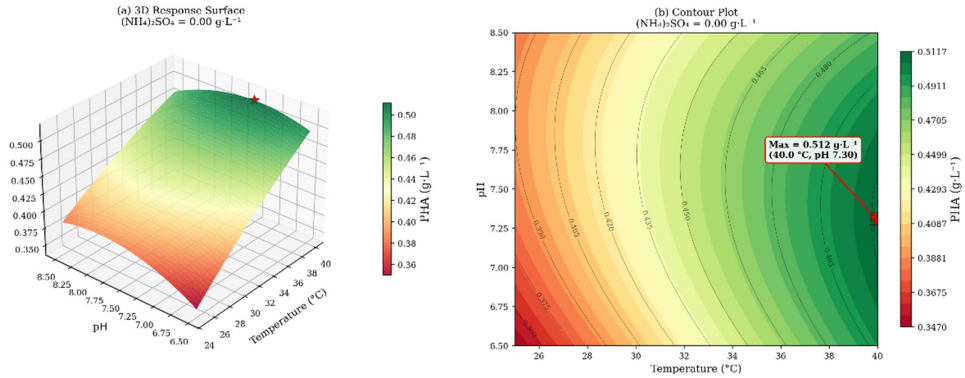

Figure 6. Three-dimensional response surface plot (a) and corresponding contour plot (b) showing the combined effects of temperature (°C) and pH on PHA concentration (g·L^{-1}) at a fixed $(NH_4)_2SO_4$ concentration of 0 g·L^{-1}. The red star indicates the predicted maximum.

Figure 7 presents the interaction between temperature and nitrogen concentration at pH 7.30. The surface reveals that the highest PHA concentrations are achieved in the region of elevated temperature, combined with the absence of external nitrogen supplementation. A notable feature is the upward curvature along the nitrogen axis, reflecting the positive quadratic coefficient for C^2 (+0.0455). This curvature indicates that within the factorial region, the response increases towards both the lower (0 g·L^{-1}) and upper (1.2 g·L^{-1}) boundaries of nitrogen concentration, with a trough near the centre point (0.6 g·L^{-1}). Nevertheless, the negative linear coefficient for C (−0.0442) ensures that

 doi:10.20944/preprints202603.2393.v1

the global maximum within the factorial cube lies at the low-nitrogen boundary, which is physiologically consistent with nitrogen limitation as a trigger for PHA biosynthesis.

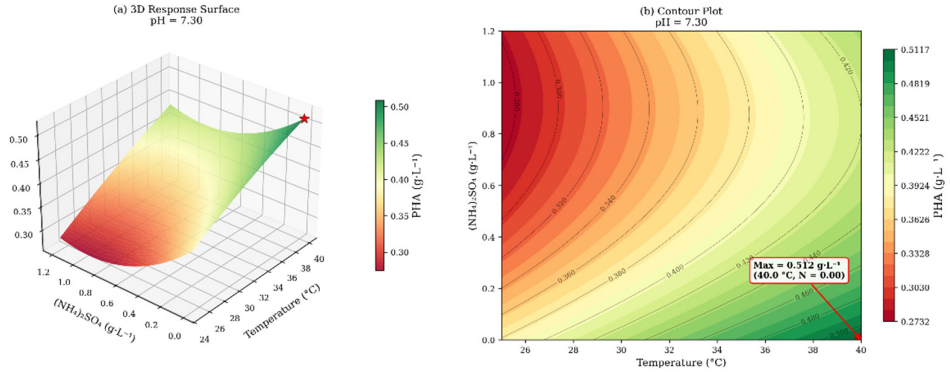

Figure 7. Three-dimensional response surface plot (a) and corresponding contour plot (b) showing the combined effects of temperature (°C) and $(NH_4)_2SO_4$ concentration (N, g·L⁻¹) on PHA concentration (g·L⁻¹) at pH 7.30. The red star indicates the predicted maximum.

Figure 8 displays the pH–nitrogen interaction at the optimal temperature of 40 °C. The response is primarily governed by the nitrogen axis, with pH exerting a secondary modulatory effect. The contour lines are elongated along the pH axis, confirming that pH has a relatively limited influence on PHA production within the range studied (6.5–8.5). This behaviour may reflect the intrinsic pH-buffering properties of the cocoa mucilage medium, which would attenuate the effect of the initial pH setpoint during fermentation.

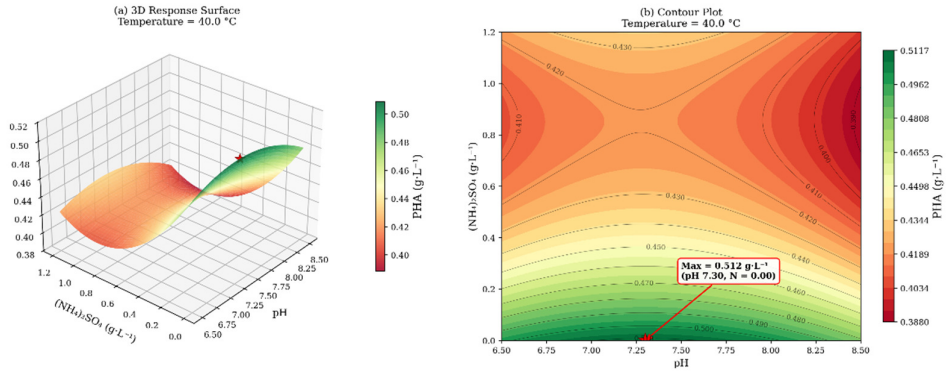

Figure 8. Three-dimensional response surface plot (a) and corresponding contour plot (b) showing the combined effects of pH and $(NH_4)_2SO_4$ concentration on PHA concentration (g·L⁻¹) within the factorial region, at a fixed temperature of 40 °C. The red star indicates the predicted maximum.

These findings align with reports on PHA biosynthesis in related *Bacillus* sensu lato species. Penkhrue et al. [78] reported that optimum PHB accumulation by *Bacillus drentensis* BP17 occurred at elevated temperatures under nitrogen-limited conditions when cultivated on pineapple peel waste. Similarly, Muneer et al. [79] observed that nitrogen-limiting conditions were essential for maximising PHA production by *Pseudomonas* sp. strains. The general metabolic rationale is that nutrient limitation, particularly of nitrogen, triggers the diversion of carbon flux from the tricarboxylic acid (TCA) cycle towards acetyl-CoA condensation and subsequent PHA polymerisation as a carbon and energy storage strategy [7,75].

 doi:10.20944/preprints202603.2393.v1

3.4.4. Numerical Optimisation and Experimental Validation

Numerical optimisation was performed to identify the combination of factor levels predicted to maximise PHA production within the factorial region of the design (coded levels −1 to +1). This constraint was deliberately imposed to ensure that the predicted optimum lies within the domain where the model has been most reliably validated by the factorial observations, rather than at the axial extremes where prediction uncertainty increases [77]. The optimisation was conducted using a multi-start L-BFGS-B algorithm implemented in the SciPy library for Python [80], with bounds set to $-1 \leq A, B, C \leq +1$.

The analysis yielded an optimum set of conditions comprising a temperature of 40 °C (A = +1.00), a pH of 7.30 (B = −0.20) and an ammonium sulphate concentration of 0 g·L−1 (C = −1.00), with a predicted PHA concentration of 0.512 g·L^{-1}. The optimal temperature coincides with the upper factorial level, while nitrogen is predicted to be most effective at its lower factorial bound, reinforcing the key role of nitrogen limitation in PHA accumulation. The predicted optimal pH of 7.30 is slightly below the design centre (7.50), consistent with the marginally negative pH–temperature interaction.

To verify the model's predictive accuracy, the prediction was compared with the experimental run that most closely matched the optimal conditions: standard order 2 (40 °C, pH 6.50, 0 g·L^{-1} nitrogen), which produced 0.496 g·L^{-1} of PHA. The model's prediction for this specific combination was 0.498 g·L^{-1}, representing a deviation of less than 0.5%. The close agreement between the model prediction at the optimum (0.512 g·L^{-1}) and the best experimental observation (0.496 g·L^{-1}) further supports the reliability of the fitted model. The diagnostic plot of predicted versus actual values (Figure 9) illustrates the close agreement between model predictions and experimental observations across the entire design space (R^2 = 0.978).

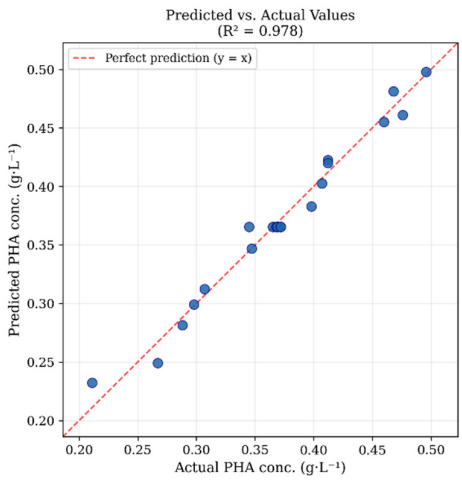

Figure 9. Diagnostic plot of predicted versus actual PHA concentration values. The dashed line represents perfect agreement (y = x). R^2 = 0.978.

Under the predicted optimal conditions, a volumetric productivity of approximately 21.3 mg·L^{-1}·h^{-1} at 24 h was estimated. To place these results in context, Table 8 presents a comparative summary of PHA production by wild-type bacterial strains cultivated on agro-industrial waste substrates under flask- or laboratory-scale conditions, as reported in the recent literature.

 doi:10.20944/preprints202603.2393.v1

Table 8. Comparison of PHA production by wild-type bacterial strains cultivated on agro-industrial waste substrates at flask or laboratory scale.

Organism	Substrate	PHA type	Time (h)	PHA ($g \cdot L^{-1}$)	*Prod.* [1] ($mg \cdot L^{-1} \cdot h^{-1}$)	Ref.
***P. aryabhattai* NBP01-UTN**	**Cocoa mucilage**	**PHB**	**24**	**0.496**	**20.7**	**This study**
B. drentensis BP17	Pineapple peel	PHB	72	0.47	6.5	[78]
Bacillus sp.	Cashew apple juice	PHA	48	0.51	10.6	[81]
B. megaterium INCQS 425	Crude glycerol (biodiesel)	PHB	72	0.78	10.8	[82,83]
R. eutropha	Cassava starch	PHB	20	0.62	31.0	[84]
B. cereus EGU3	Glucose	PHB	20	0.50	25.0	[85]
B. megaterium LVN01	Biogas digestate	PHBV	–	0.36	–	[86]
Bacillus sp. SV13	Pineapple + sugarcane waste	PHB	48	1.86	38.8	[75]
Pseudomonas sp. AK-3	Molasses	PHA	24	0.21	8.8	[79]
B. cereus S3	Cocoa pod husk (7% w/v)	PHA	48	–	–	[87–89]

[1] *Prod.*, volumetric productivity. Values marked '–' were not reported in the original study.

As shown in Table 8, the maximum PHA concentration achieved in this study (0.496 $g \cdot L^{-1}$) is within the same order of magnitude as those reported for other wild-type strains cultivated on agro-industrial waste substrates at laboratory scale. The volumetric productivity (20.7 $mg \cdot L^{-1} \cdot h^{-1}$) is notably competitive, largely attributable to a shorter fermentation time of 24 h compared with the 48–72 h used in several cited studies. For instance, *B. drentensis* BP17 required 72 h to produce 0.47 $g \cdot L^{-1}$ of PHB from pineapple peel [78], yielding a volumetric productivity approximately three-fold lower than that achieved here. Similarly, de Jesus Assis et al. [82] reported 0.78 $g \cdot L^{-1}$ with *B. megaterium* INCQS 425 on crude glycerol, but over 72 h (productivity ≈10.8 $mg \cdot L^{-1} \cdot h^{-1}$). The study by *Bacillus* sp. SV13 on pineapple and sugarcane waste achieved a notably higher titre (1.86 $g \cdot L^{-1}$) [75], reflecting the benefit of a richer mixed-waste substrate. It is also noteworthy that Ismail and Hameed [88,89] employed cocoa pod husk as substrate for *B. cereus* PHA production, confirming the broader potential of cacao-derived residues as fermentation feedstocks.

It should be noted that the PHA concentrations reported herein were obtained under non-sterile, laboratory-scale conditions during a pandemic, which imposed practical constraints on the available fermentation infrastructure. Notwithstanding these limitations, the results demonstrate that cocoa mucilage can serve as a viable and cost-effective carbon source for PHA production by *P. aryabhattai*, and suggest that further improvements in yield may be achievable through process intensification strategies such as fed-batch operation, controlled dissolved oxygen management and medium supplementation with trace elements [72,75].

From a process economics perspective, the finding that maximal PHA production was achieved without any external nitrogen supplementation is particularly noteworthy. The endogenous nitrogen content in cocoa mucilage appears sufficient to sustain bacterial growth while simultaneously creating the nutrient imbalance required to trigger PHA biosynthesis. This observation has favourable implications for the cost-effectiveness of the proposed bioprocess, as nitrogen sources typically represent a significant fraction of the total fermentation medium cost in industrial PHA production [8,90]. Furthermore, the use of open-source statistical tools (*Python/statsmodels/SciPy*) in lieu of proprietary software ensures full reproducibility of the analysis; the complete computational script is provided as Supplementary Material S1.

 doi:10.20944/preprints202603.2393.v1

3.5. Characterisation of the Produced PHA

3.5.1. Fourier-Transform Infrared Spectroscopy (FTIR)

The chemical identity of the biopolymer extracted from *P. aryabhattai* NBP01-UTN was investigated by FTIR spectroscopy in transmittance mode (400–4000 cm^{-1}, resolution 4 cm^{-1}, 8 sample scans, Happ–Genzel apodisation) using an Agilent Cary 630 spectrometer equipped with a diamond ATR accessory. Two independent extracts from the fermentation under optimised conditions were analysed (samples M2B and M2B2). The resulting spectra, which were highly reproducible between the two preparations, are presented in Figure 10; the principal absorption bands and their assignments are summarised in Table 9.

The spectra exhibited a set of absorption bands that, taken together, constitute a diagnostic fingerprint for polyhydroxyalkanoates. Five spectral features are of particular significance for polymer identification.

i. A broad absorption band centred near 3440 cm^{-1} was attributable to O–H stretching vibrations. In the context of a PHA extracted by chloroform dissolution, this band most likely arises from terminal hydroxyl groups at the carboxyl end of the polymer chains, with possible contributions from residual moisture adsorbed during sample preparation. Its moderate intensity relative to the dominant ester bands indicates that the extracted material is predominantly polymeric rather than oligomeric, since short-chain PHAs exhibit proportionally stronger hydroxyl absorption [91,92].

ii. Two absorption bands in the 2970–2850 cm^{-1} region corresponded to the asymmetric and symmetric C–H stretching vibrations of methyl (CH_3) and methylene (CH_2) groups. These bands arise from the aliphatic repeat unit of the PHA backbone (–O–CH(CH_3)–CH_2–CO–) and are a universal feature of all short-chain-length (scl) PHAs [47,91]. Their moderate intensity compared to the carbonyl band is characteristic of PHB, in which each repeat unit contains only one methyl and one methylene group.

iii. The most diagnostically significant feature was a strong, sharp absorption band in the region of 1720–1740 cm^{-1}, corresponding to the C=O stretching vibration of the ester carbonyl group. This band is universally recognised as the primary spectroscopic marker for PHA identification, as it originates from the repeating ester linkage that defines the polymer backbone [47,82,91]. In crystalline PHB, this band is typically centred near 1720–1726 cm^{-1}, whereas in amorphous or molten PHB it shifts to approximately 1740 cm^{-1} owing to the loss of inter-chain interactions within the crystalline lattice [93,94]. The position of this band in the present spectra is therefore informative regarding the degree of crystallinity of the extracted material. Its high intensity—the strongest absorption in the entire spectrum—confirms that the ester functional group is the dominant structural motif, consistent with a high-molecular-weight polyester.

iv. Bands in the 1450–1380 cm^{-1} region were assigned to C–H bending (deformation) modes of the CH_3 and CH_2 groups. In crystalline PHB, the symmetric CH_3 bending mode near 1380 cm^{-1} can appear as a doublet reflecting the conformational order of the 21 helical chain packing in the orthorhombic unit cell [93]. Whether such a doublet is resolved in the present spectra would require higher spectral resolution or band-fitting analysis, but the presence of absorption in this region is consistent with PHA.

v. A cluster of strong absorption bands in the 1280–1050 cm^{-1} region was assigned to C–O–C stretching vibrations of the ester linkage. This region constitutes the second most informative spectral window for PHA identification after the carbonyl band. The band near 1280 cm^{-1} has been specifically associated with the helical conformation adopted by crystalline PHB chains [93,95], and its presence provides additional evidence of a semi-crystalline polymer structure. Bands below 1000 cm^{-1} were attributed to C–C skeletal stretching and various backbone deformation modes.

The overall spectral pattern is in close agreement with FTIR spectra reported for PHB produced by *Bacillus* sensu lato species. Penkhrue et al. [96] reported analogous bands for PHB from *B.*

 doi:10.20944/preprints202603.2393.v1

drentensis BP17 (C=O at 1720 cm^{-1}, C–O–C at 1000–1300 cm^{-1}), and Muneer et al. [97] identified the ester carbonyl at 1728 cm^{-1} as the primary diagnostic feature in PHAs from novel bacterial isolates. De Apati et al. [82] further demonstrated that the relative intensity ratio between the carbonyl band and the C–H stretching bands can serve as a semi-quantitative indicator of PHA purity. The consistency of the present spectra with these published references provides strong evidence that the biopolymer produced from cocoa mucilage is a member of the PHA family, most likely PHB or a PHB-dominant copolymer.

Table 9. Principal FTIR absorption bands and their assignments for the PHA extracted from *Priestia aryabhattai* NBP01-UTN.

Wavenumber (cm^{-1})	Assignment	Interpretation
~3440	O–H stretching	Terminal hydroxyl groups; residual moisture
~2970–2930	C–H asym. stretching (CH_3, CH_2)	Aliphatic backbone of PHA repeat unit
~2850	C–H sym. stretching (CH_2)	Methylene groups in the main chain
~1720–1740	C=O stretching (ester carbonyl)	Diagnostic PHA marker. ~1720 cm^{-1} crystalline; ~1740 cm^{-1} amorphous
~1450	δ(CH_3) asym. bending	Methyl deformation
~1380	δ(CH_3) sym. bending	Methyl 'umbrella' mode; crystallinity-sensitive in PHB
~1280	C–O–C stretching	Coupled C–C; helical conformation marker in crystalline PHB
~1130–1050	C–O–C asym. stretching	Ester bond vibrations characteristic of PHA
~980–800	C–C skeletal / C–O stretching	Backbone deformation; fingerprint region

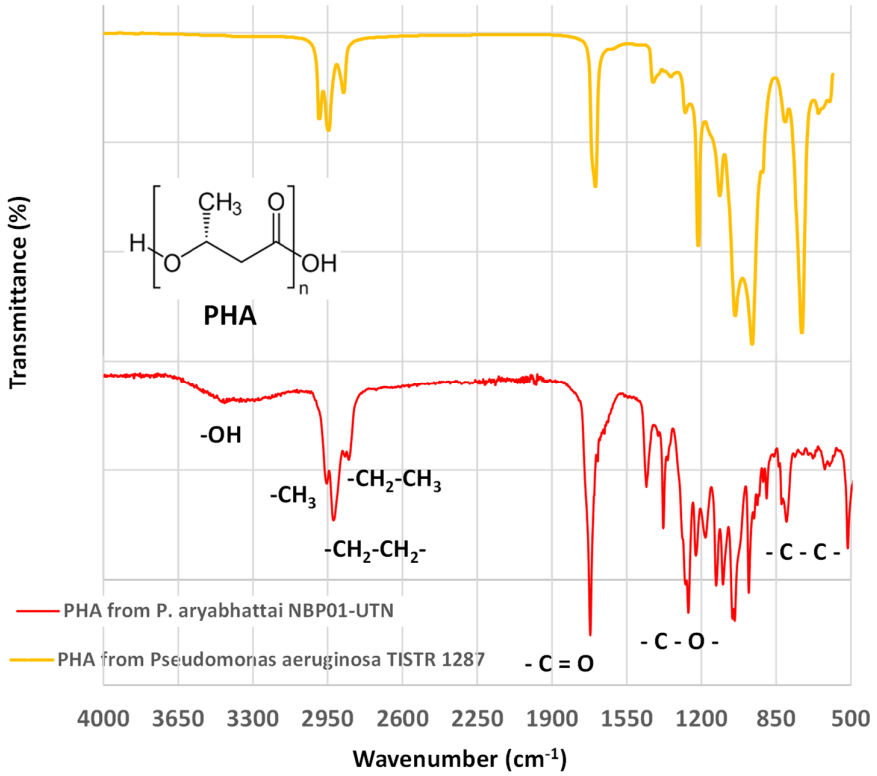

Figure 10. FTIR spectra (transmittance mode, 4000–500 cm^{-1}) of the PHA extracted from *Priestia aryabhattai* NBP01-UTN (red) compared with the PHA produced by *Pseudomonas aeruginosa* TISTR 1287 (yellow) [98]. The

 doi:10.20944/preprints202603.2393.v1

principal absorption bands corresponding to the characteristic functional groups of polyhydroxyalkanoates are indicated. Inset: general chemical structure of the PHA repeating unit.

3.5.2. Differential Scanning Calorimetry (DSC)

The thermal behaviour of the extracted PHA was investigated by differential scanning calorimetry (DSC) using a Setaram DSC 131 Evo instrument (Setaram Instrumentation, Caluire, France) at Yachay Tech University. The sample was subjected to a controlled heating programme from −20 to 250 °C under a nitrogen atmosphere and at a heating rate of 10 °C/min. The resulting thermogram is presented in Figure 11, and the principal thermal events are summarised in Table 10.

A first notable observation is the absence of a detectable glass transition (Tg) step in the heating thermogram. For PHB, Tg is typically reported in the range of 0–5 °C [99,100], and its detection requires a sufficient proportion of amorphous material to produce a measurable change in heat capacity. The absence of a discernible Tg step strongly suggests that the extracted polymer possesses a high degree of crystallinity, leaving an amorphous fraction too small to generate a detectable calorimetric signal. This inference is consistent with the behaviour reported by Barham et al. [99] for melt-crystallised PHB, where Tg becomes undetectable at crystallinity levels exceeding approximately 60%. In polymer processing, high crystallinity also explains the brittle, rigid character typically observed when handling PHB films.

The most prominent features of the thermogram were two well-resolved endothermic peaks at 144.5 °C (Tm1) and 164.2 °C (Tm2), with a melting onset temperature of approximately 125 °C. The higher-temperature peak was the most intense of the two (peak height ratio Tm2/Tm1 ≈ 1.43), indicating that the majority of the crystalline mass melts at the higher temperature. This double-melting behaviour is a well-documented and highly characteristic feature of PHB, and has been the subject of extensive investigation in the polymer physics literature [99,101,102].

The accepted explanation for this phenomenon is the melt–recrystallisation–remelt mechanism: during the heating scan, smaller or less thermodynamically stable crystallites melt first, producing the lower endotherm at Tm1. The polymer chains released by this initial melting undergo rapid in situ recrystallisation into more perfect crystalline lamellae, which subsequently melt at the higher temperature Tm2 [99,101]. Evidence for this intermediate recrystallisation is provided by the shallow exothermic trough observed at approximately 150 °C between the two endothermic peaks, which corresponds to the heat released during the reorganisation process. The dominance of the Tm2 peak (height ratio 1.43) indicates that a substantial proportion of the material undergoes this reorganisation, consistent with a polymer containing a broad distribution of crystallite perfection—as might be expected for PHA accumulated intracellularly under dynamic fermentation conditions.

The principal melting temperature Tm2 = 164.2 °C falls within the lower portion of the range commonly reported for PHB homopolymer (160–180 °C) [75,99–101]. Several factors could account for this: (a) a relatively low molecular weight, which reduces the thermodynamic melting point; (b) the presence of residual impurities co-extracted with the polymer, which can act as diluents and depress Tm; or (c) the possible incorporation of minor proportions of 3-hydroxyvalerate (3HV) or other co-monomer units, which are known to lower the melting point of the crystalline PHB phase even at low molar fractions [100,103]. Distinguishing among these possibilities would require complementary techniques such as gel permeation chromatography (for molecular weight) or gas chromatography–mass spectrometry and/or NMR spectroscopy (for monomer composition), which are recommended for future work.

Beyond the melting region, the thermogram exhibited a continuously rising heat-flow signal from approximately 200 °C onwards, with an inflexion point near 221 °C. This feature marks the onset of thermal decomposition (Td). The thermal degradation of PHB proceeds predominantly via a β-elimination (cis-elimination) mechanism involving a six-membered-ring transition state, yielding crotonic acid and oligomers with crotonate end groups as the primary degradation products [104,105]. Since the DSC scan was terminated at 250 °C, the full decomposition peak was not captured;

 doi:10.20944/preprints202603.2393.v1

however, the decomposition onset near 221 °C is consistent with values reported for PHB (typically 220–300 °C) [99,100,104].

The relatively narrow processing window between the principal melting temperature and the decomposition onset (Td − Tm2 ≈ 57 °C) is a well-known limitation of PHB, constraining conventional melt-processing operations such as extrusion and injection moulding [100,104]. This narrow window has been one of the principal motivations for developing PHA copolymers with broader processing ranges [75,103].

The thermal properties determined for the PHA produced by *P. aryabhattai* NBP01-UTN (Tm ≈ 164 °C, Td onset ≈ 221 °C, undetectable Tg) are consistent with values reported for PHB from related species. Penkhrue et al. [106] reported Tm = 175 °C for PHB from *B. drentensis*, while Muneer et al. [79] observed Tm values of 158–170 °C for PHA from various bacterial isolates. The somewhat lower Tm in the present study may reflect the extraction conditions or a less pure extract, consistent with the constraints under which the fermentation was conducted.

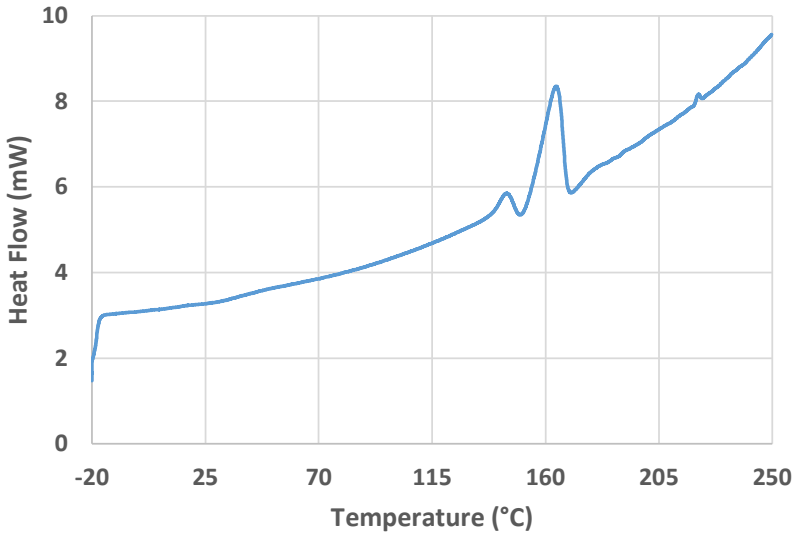

Figure 11. DSC thermogram (heating scan, −20 to 250 °C) of the PHA extracted from *P. aryabhattai* NBP01-UTN. Endothermic events are oriented upward. T~m1~ = 144.4 °C (ΔH~m1~ = 8.5 J/g); T~m2~ = 164.2 °C (ΔH~m2~ = 36.8 J/g); T~d,onset~ ≈ 221 °C.

Table 10. Summary of the principal thermal events identified in the DSC thermogram of the PHA extracted from *P. aryabhattai* NBP01-UTN.

Thermal Event	T (°C)	Type	Interpretation
Glass transition (Tg)	Not detected	–	Absence suggests high crystallinity
Melting onset	~122 (X1)	Endothermic onset	Beginning of crystallite melting
Melting peak I (Tm_1)	144.4	Endothermic peak	Melting of less perfect crystallites
Recrystallisation trough	150.0	Exothermic dip	In situ melt–recrystallisation
Melting peak II (Tm_2)	164.2	Endothermic peak (major)	Melting of reorganised, more perfect crystallites
Decomposition onset (Td)	~221	Endothermic (rising)	β-elimination chain scission; peak beyond scan range

3.5.3. Integrated Assessment of Polymer Identity

The combined evidence from three independent analytical techniques converges on the identification of the biopolymer produced by *P. aryabhattai* NBP01-UTN from cocoa mucilage as a polyhydroxyalkanoate, most likely poly(3-hydroxybutyrate) (PHB) or a PHB-rich copolymer. The

 doi:10.20944/preprints202603.2393.v1

evidence is summarised as follows: (i) the FTIR spectrum exhibited the diagnostic ester carbonyl band near 1720–1740 cm^{-1} together with characteristic C–H and C–O–C absorption bands, all consistent with the spectral fingerprint of scl-PHAs reported in the literature; (ii) the DSC thermogram displayed a double-melting endotherm (Tm1 = 144.4 °C, Tm2 = 164.2 °C) attributable to the melt–recrystallisation–remelt mechanism characteristic of PHB, an undetectable Tg consistent with high crystallinity, and a decomposition onset near 221 °C consistent with β-elimination degradation of PHB; and (iii) the Sudan Black B spectrophotometric assay confirmed abundant intracellular lipophilic granules characteristic of PHA accumulation.

It should be acknowledged that a definitive determination of the monomer composition would require gas chromatography–mass spectrometry (GC–MS) or 1H/13C nuclear magnetic resonance (NMR) spectroscopy. These techniques would permit unambiguous confirmation of whether the polymer is a PHB homopolymer or a copolymer containing minor proportions of other hydroxyalkanoate monomers (e.g., 3HV), and would also enable estimation of the number-average molecular weight. Such analyses are recommended as priorities for future work to complement the structural characterisation presented herein.

5. Conclusions

This study demonstrated the feasibility of producing polyhydroxyalkanoates from cocoa mucilage, an underutilised agro-industrial by-product of the Ecuadorian cacao sector, using a wild-type *Priestia aryabhattai* strain isolated directly from cocoa fruit residues. The principal findings and contributions of this work are as follows.

A screening programme based on Sudan Black B staining and UV–Vis spectrophotometric confirmation identified one PHA-producing isolate (strain NBP01-UTN) among four morphologically distinct microbial types recovered from cocoa fruit residues. Molecular identification by 16S rRNA gene sequencing and phylogenetic analysis assigned this isolate to *Priestia aryabhattai*, representing, to the best of the authors' knowledge, the first report of a PHA-producing strain of this species isolated from cocoa (Theobroma cacao L.) fruit residues.

The physicochemical characterisation of raw cocoa mucilage confirmed its suitability as a fermentation substrate, with a total reducing sugar content of 12.20 ± 0.72% (m/v), free glucose of 4.97 ± 0.21% (m/v) and an acidic pH of 3.70 ± 0.05. A simple two-step preparation protocol—dilution to 50% (v/v) followed by pH adjustment with NaOH—was sufficient to render the mucilage suitable for bacterial fermentation without the need for costly pre-treatment or supplementation.

Optimisation of the submerged fermentation conditions by response surface methodology with a central composite design yielded a highly significant quadratic model (R^2 = 0.978, $p < 0.0001$) that identified temperature and nitrogen source concentration as the dominant factors influencing PHA biosynthesis. The predicted optimal conditions—40 °C, pH 7.30 and 0 $g \cdot L^{-1}$ ammonium sulphate—yielded a maximum PHA concentration of 0.496 $g \cdot L^{-1}$ at 24 h, corresponding to a volumetric productivity of approximately 20.7 $mg \cdot L^{-1} \cdot h^{-1}$. Notably, the finding that maximal PHA production was achieved without external nitrogen supplementation is of particular significance from a process economics perspective, as the endogenous nitrogen content of cocoa mucilage alone was sufficient to sustain the nutrient imbalance required for polymer accumulation.

The structural and thermal characterisation of the extracted polymer by FTIR spectroscopy and DSC provided converging evidence consistent with poly(3-hydroxybutyrate) (PHB) or a PHB-dominant copolymer. The FTIR spectra exhibited the diagnostic ester carbonyl band near 1720–1740 cm^{-1} together with characteristic C–H and C–O–C absorption bands, whilst the DSC thermogram displayed a double-melting endotherm (Tm1 = 144.5 °C; Tm2 = 164.2 °C) attributable to the melt–recrystallisation–remelt mechanism characteristic of PHB, an undetectable glass transition temperature indicative of high crystallinity, and a thermal decomposition onset near 221 °C.

Whilst the PHA yields reported herein are modest compared with those achievable by engineered strains under optimised industrial conditions, the volumetric productivity is competitive with values reported for other wild-type organisms cultivated on agro-industrial waste substrates at

 doi:10.20944/preprints202603.2393.v1

laboratory scale. It should be acknowledged that a definitive determination of the monomer composition would require complementary techniques such as gas chromatography–mass spectrometry (GC–MS) or nuclear magnetic resonance (NMR) spectroscopy, and that validation of the optimised conditions at pilot scale remains necessary before translation to industrial application.

In a broader context, this work contributes to the valorisation of cocoa agro-industrial waste within a circular bioeconomy framework, demonstrating that coupling a locally isolated wild-type strain with a locally abundant, low-cost substrate is a viable strategy for bioplastic production. Future research priorities should include determining the polymer's monomer composition and molecular weight by GC–MS and/or NMR, evaluating fed-batch and continuous fermentation strategies to enhance productivity, and assessing the techno-economic feasibility of the proposed bioprocess at pilot scale.

Supplementary Materials: The following supporting information can be downloaded at the website of this paper posted on Preprints.org.

Author Contributions: Conceptualisation, J.N.P. and J.M.P.C.; methodology, J.N.P. and O.J.C.L.; software, J.N.P., J.M.P.C.; validation, R.C.E.V. and P.B.; formal analysis, P.B., H.M.R.C..; investigation, J.N.P., O.J.C.L., P.B.; resources, O.J.C.L., R.C.E.V.; data curation, P.B.; writing—original draft preparation, J.N.P., O.J.C.L.; writing—review and editing, J.M.P.C.; visualisation, J.M.P.C.; supervision, R.C.E.V.; project administration, J.N.P., O.J.C.L.; funding acquisition, O.J.C.L., R.C.E.V. All authors have read and agreed to the published version of the manuscript.

Funding: Please add: This research received no external funding.

Acknowledgments: The authors would like to express their gratitude to our esteemed Rector, Miguel Naranjo Toro, for their support of this research. Generative artificial intelligence was employed to prepare the Graphical Abstract and to review English grammar.

Conflicts of Interest: The authors declare no conflicts of interest.

Abbreviations

The following abbreviations are used in this manuscript:

3HB	3-Hydroxybutyrate
3HV	3-Hydroxyvalerate
ANI	Average nucleotide identity
ANOVA	Analysis of variance
AOAC	Association of Official Analytical Chemists
ATR	Attenuated total reflectance
BLASTn	Basic Local Alignment Search Tool (nucleotide)
CCD	Central composite design
CSI	Conserved signature indel
C.V.	Coefficient of variation
DNA	Deoxyribonucleic acid
DNS	3,5-Dinitrosalicylic acid
DSC	Differential scanning calorimetry
DTA	Differential thermal analysis
FTIR	Fourier-transform infrared spectroscopy
GC–MS	Gas chromatography–mass spectrometry
GOD-PAP	Glucose oxidase–peroxidase
L-BFGS-B	Limited-memory Broyden–Fletcher–Goldfarb–Shanno (bound-constrained)
MEGA	Molecular Evolutionary Genetics Analysis
NCBI	National Centre for Biotechnology Information
NMR	Nuclear magnetic resonance
OLS	Ordinary least squares
PCR	Polymerase chain reaction
PHA(s)	Polyhydroxyalkanoate(s)

 doi:10.20944/preprints202603.2393.v1

PHB	Poly(3-hydroxybutyrate)
PHBV	Poly(3-hydroxybutyrate-co-3-hydroxyvalerate)
PRESS	Predicted residual error sum of squares
rRNA	Ribosomal ribonucleic acid
RSM	Response surface methodology
scl	Short-chain-length
SD	Standard deviation
TCA	Tricarboxylic acid
UTN	Universidad Técnica del Norte
UV–Vis	Ultraviolet–visible
WCB	Working cell bank

References

1. Plastics—the Fast Facts 2023 • Plastics Europe Available online: https://plasticseurope.org/knowledge-hub/plastics-the-fast-facts-2023/ (accessed on 15 March 2026).
2. Ali, S.S.; Abdelkarim, E.A.; Elsamahy, T.; Al-Tohamy, R.; Li, F.; Kornaros, M.; Zuorro, A.; Zhu, D.; Sun, J. Bioplastic Production in Terms of Life Cycle Assessment: A State-of-the-Art Review. *Environmental Science and Ecotechnology* **2023**, *15*, 100254, doi:10.1016/j.ese.2023.100254.
3. Costa, A.; Encarnação, T.; Tavares, R.; Todo Bom, T.; Mateus, A. Bioplastics: Innovation for Green Transition. *Polymers 2023, Vol. 15*, **2023**, *15*, doi:10.3390/polym15030517.
4. Getino, L.; Martín, J.L.; Chamizo-Ampudia, A. A Review of Polyhydroxyalkanoates: Characterization, Production, and Application from Waste. *Microorganisms 2024, Vol. 12*, **2024**, *12*, doi:10.3390/microorganisms12102028.
5. Colombo, B.; Sciarria, T.P.; Reis, M.; Scaglia, B.; Adani, F. Polyhydroxyalkanoates (PHAs) Production from Fermented Cheese Whey by Using a Mixed Microbial Culture. *Bioresour. Technol.* **2016**, *218*, 692–699, doi:10.1016/j.biortech.2016.07.024.
6. Koller, M.; Mukherjee, A. A New Wave of Industrialization of PHA Biopolyesters. *Bioengineering 2022, Vol. 9*, **2022**, *9*, doi:10.3390/bioengineering9020074.
7. Muneer, F.; Rasul, I.; Azeem, F.; Siddique, M.H.; Zubair, M.; Nadeem, H. Microbial Polyhydroxyalkanoates (PHAs): Efficient Replacement of Synthetic Polymers. *Journal of Polymers and the Environment 2020 28:9* **2020**, *28*, 2301–2323, doi:10.1007/s10924-020-01772-1.
8. Rodriguez-Perez, S.; Serrano, A.; Pantión, A.A.; Alonso-Fariñas, B. Challenges of Scaling-up PHA Production from Waste Streams. A Review. *J. Environ. Manage.* **2018**, *205*, 215–230, doi:10.1016/j.jenvman.2017.09.083.
9. Chavan, S.; Yadav, B.; Tyagi, R.D.; Drogui, P. A Review on Production of Polyhydroxyalkanoate (PHA) Biopolyesters by Thermophilic Microbes Using Waste Feedstocks. *Bioresour. Technol.* **2021**, *341*, 125900, doi:10.1016/j.biortech.2021.125900.
10. Chavan, S.; Yadav, B.; Tyagi, R.D.; Drogui, P. A Review on Production of Polyhydroxyalkanoate (PHA) Biopolyesters by Thermophilic Microbes Using Waste Feedstocks. *Bioresour. Technol.* **2021**, *341*, 125900, doi:10.1016/j.biortech.2021.125900.
11. Kanzariya, R.; Gautam, A.; Parikh, S.; Shah, M.; Gautam, S. Formation of Polyhydroxyalkanoates Using Agro and Industrial Waste as a Substrate–a Review. *Biotechnol. Genet. Eng. Rev.* **2023**, *39*, 897–936, doi:10.1080/02648725.2023.2165222.
12. Arriaga, M.; Pinar, F.J.; Izarra, I.; Amo, J. del; Vicente, J.; Fernández-Morales, F.J.; Mena, J. Valorization of Agri-Food Waste into PHA and Bioplastics: From Waste Selection to Transformation. *Applied Sciences 2025, Vol. 15*, **2025**, *15*, doi:10.3390/app15031008.
13. Sehgal, R.; Kumar, A.; Gupta, R. Bioconversion of Rice Husk as a Potential Feedstock for Fermentation by Priestia Megaterium POD1 for the Production of Polyhydroxyalkanoate. *Waste and Biomass Valorization 2023 14:11* **2023**, *14*, 3657–3670, doi:10.1007/s12649-023-02039-1.
14. Jarrín-Chacón, J.P.; Núñez-Pérez, J.; Espín-Valladares, R. del C.; Manosalvas-Quiroz, L.A.; Rodríguez-Cabrera, H.M.; Pais-Chanfrau, J.M. Pectin Extraction from Residues of the Cocoa Fruit (Theobroma Cacao L.) by Different Organic Acids: A Comparative Study. *Foods* **2023**, *12*, doi:10.3390/FOODS12030590.

 doi:10.20944/preprints202603.2393.v1

15. ICCO Releases Its First Forecast for the 2023/24 Cocoa Year Available online: https://www.comunicaffe.com/icco-releases-its-first-forecast-for-the-2023-24-cocoa-year/ (accessed on 15 March 2026).
16. Morales, S.H.S.; Moreno, J.A.J.; Contieri, L.S.; Rostagno, M.A.; Forster-Carneiro, T. Cocoa Waste Valorization: A Review and Sustainability Analysis of Green Technologies. *Biofuels, Bioproducts and Biorefining* **2025**, *19*, 2680–2699, doi:10.1002/bbb.70029.
17. Arvelo Sánchez, M.Á.; Delgado, T.; Maroto, S.; Rivera, J.; Higuera, I.; Navarro, A. Estado Actual Sobre La Producción y El Comercio Del Cacao En América. **2016**.
18. Gupta, R.S.; Patel, S.; Saini, N.; Chen, S. Robust Demarcation of 17 Distinct Bacillus Species Clades, Proposed as Novel Bacillaceae Genera, by Phylogenomics and Comparative Genomic Analyses: Description of Robertmurraya Kyonggiensis Sp. Nov. and Proposal for an Emended Genus Bacillus Limiting It …. *Int. J. Syst. Evol. Microbiol.* **2020**, *70*, 5753–5798, doi:10.1099/ijsem.0.004475.
19. Biedendieck, R.; Knuuti, T.; Moore, S.J.; Jahn, D. The "Beauty in the Beast"—the Multiple Uses of Priestia Megaterium in Biotechnology. *Applied Microbiology and Biotechnology 2021 105:14* **2021**, *105*, 5719–5737, doi:10.1007/s00253-021-11424-6.
20. Chathalingath, N.; Kingsly, J.S.; Gunasekar, A. Biosynthesis and Biodegradation of Poly(3-Hydroxybutyrate) from Priestia Flexa; A Promising Mangrove Halophyte towards the Development of Sustainable Eco-Friendly Bioplastics. *Microbiol. Res.* **2023**, *267*, 127270, doi:10.1016/j.micres.2022.127270.
21. Rysbek, A.; Jankiewicz, U.; Pogorzelska-Nowicka, E.; Wyrwisz, J.; Abeldenov, S.; Mirończuk, A.M.; Richert, A. Evaluation of the Method of Periodic Medium Renewal of Bacillus Aryabhattai RAF 5 and Analysis of P(3HB) Production. *Polymers 2025, Vol. 17*, **2025**, *17*, doi:10.3390/polym17070968.
22. Cal, A.J.; Chan, V.J.; Luo, W.K.; Lee, C.C. Polyhydroxyalkanoate Production in Priestia Megaterium Strains from Glycerol Feedstock. *PLoS One* **2025**, *20*, e0322838, doi:10.1371/journal.pone.0322838.
23. Sehgal, R.; Kumar, A.; Gupta, R. Bioconversion of Rice Husk as a Potential Feedstock for Fermentation by Priestia Megaterium POD1 for the Production of Polyhydroxyalkanoate. *Waste and Biomass Valorization 2023 14:11* **2023**, *14*, 3657–3670, doi:10.1007/s12649-023-02039-1.
24. Shahid, S.; Mosrati, R.; Corroler, D.; Amiel, C.; Gaillard, J.L. Bioconversion of Glycerol into Polyhydroxyalkanoates through an Atypical Metabolism Shift Using Priestia Megaterium during Fermentation Processes: A Statistical Analysis of Carbon and Nitrogen Source Concentrations. *Int. J. Biol. Macromol.* **2024**, *256*, 128116, doi:10.1016/j.ijbiomac.2023.128116.
25. Porras, M.A.; Villar, M.A.; Cubitto, M.A. Improved Intracellular PHA Determinations with Novel Spectrophotometric Quantification Methodologies Based on Sudan Black Dye. *J. Microbiol. Methods* **2018**, *148*, 1–11, doi:10.1016/j.mimet.2018.03.008.
26. Moreno, S.A.S.; Montoya, M.A.M.; Martínez, A.L.M.; Pérez, M. del S.Y.; https://dialnet.unirioja.es/servlet/autor?codigo=3187313; https://dialnet.unirioja.es/servlet/autor?codigo=3187314; https://dialnet.unirioja.es/servlet/autor?codigo=3187315; https://dialnet.unirioja.es/servlet/autor?codigo=2020540 Identificación de Bacterias Productoras de Polihidroxialcanoatos (PHAs) En Suelos Contaminados Con Desechos de Fique. *Revista Colombiana de Biotecnología, ISSN 0123-3475, ISSN-e 1909-8758, Vol. 14, Nº. 2, 2012, págs. 89-100* **2012**, *14*, 89–100.
27. Bergey's Manual of Systematics of Archaea and Bacteria | Wiley Available online: https://www.wiley.com/en-us/Bergey's+Manual+of+Systematics+of+Archaea+and+Bacteria-p-9781118960608 (accessed on 19 March 2026).
28. Chouhan, A.; Tiwari, A. Production of Polyhydroxyalkanoate (PHA) Biopolymer from Crop Residue Using Bacteria as an Alternative to Plastics: A Review. *RSC Adv.* **2025**, *15*, 11845–11862, doi:10.1039/d4ra08505a.
29. Naitam, M.G.; Tomar, G.S.; Kaushik, R.; Singh, S.; Nain, L. Agro-Industrial Waste as Potential Renewable Feedstock for Biopolymer Poly-Hydroxyalkanoates (PHA) Production. *Enzyme Engineering* **2022**, *11*, 1–16, doi:10.35841/2329-6674.22.11.190.
30. Asiri, F.; Chu, K.H. Valorization of Agro-Industrial Wastes into Polyhydroxyalkanoates-Rich Single-Cell Proteins to Enable a Circular Waste-to-Feed Economy. *Chemosphere* **2022**, *309*, 136660, doi:10.1016/j.chemosphere.2022.136660.

 doi:10.20944/preprints202603.2393.v1

31. Cristea, A.; Baricz, A.; Leopold, N.; Floare, C.G.; Borodi, G.; Kacso, I.; Tripon, S.; Bulzu, P.A.; Andrei, A.; Cadar, O.; et al. Polyhydroxybutyrate Production by an Extremely Halotolerant Halomonas Elongata Strain Isolated from the Hypersaline Meromictic Fără Fund Lake (Transylvanian Basin, Romania). *J. Appl. Microbiol.* **2018**, *125*, 1343–1357, doi:10.1111/jam.14029.
32. Hendy, M.H.; Shehabeldine, A.M.; Hashem, A.H.; El-Sayed, A.F.; El-Sheikh, H.H. Optimization and Characterization of Polyhydroxybutyrate Produced by Halomonas Meridiana Using Orange Peel Waste. *BMC Microbiology 2025 25:1* **2025**, *25*, 304-, doi:10.1186/s12866-025-04007-2.
33. Assia, M.; Hasnaa, A.; Sara, M.; Jamal, M.; Mohammed, M. Physico-Chemical Characterization of a Pink Red-like Pigments Produced by Five New Bacterial Soil Strains Identified as *Streptomyces Coelicoflavus*. *Am. J. Microbiol. Res.* **2018**, *6*, 67–72, doi:10.12691/ajmr-6-3-1.
34. Altschul, S.F.; Gish, W.; Miller, W.; Myers, E.W.; Lipman, D.J. Basic Local Alignment Search Tool. *J. Mol. Biol.* **1990**, *215*, 403–410, doi:10.1016/S0022-2836(05)80360-2.
35. Thompson, J.D.; Higgins, D.G.; Gibson, T.J. CLUSTAL W: Improving the Sensitivity of Progressive Multiple Sequence Alignment through Sequence Weighting, Position-Specific Gap Penalties and Weight Matrix Choice. *Nucleic Acids Res.* **1994**, *22*, 4673–4680, doi:10.1093/nar/22.22.4673.
36. Tamura, K.; Stecher, G.; Kumar, S. MEGA11: Molecular Evolutionary Genetics Analysis Version 11. *Mol. Biol. Evol.* **2021**, *38*, 3022–3027, doi:10.1093/molbev/msab120.
37. Saitou, N.; Nei, M. The Neighbor-Joining Method: A New Method for Reconstructing Phylogenetic Trees. *Mol. Biol. Evol.* **1987**, *4*, 406–425, doi:10.1093/oxfordjournals.molbev.a040454.
38. Kimura, M. A Simple Method for Estimating Evolutionary Rates of Base Substitutions through Comparative Studies of Nucleotide Sequences. *J. Mol. Evol.* **1980**, *16*, 111–120, doi:10.1007/BF01731581.
39. Felsenstein, J. CONFIDENCE LIMITS ON PHYLOGENIES: AN APPROACH USING THE BOOTSTRAP. *Evolution (N. Y).* **1985**, *39*, 783–791, doi:10.1111/j.1558-5646.1985.tb00420.x.
40. Gupta, R.S.; Patel, S.; Saini, N.; Chen, S. Robust Demarcation of 17 Distinct Bacillus Species Clades, Proposed as Novel Bacillaceae Genera, by Phylogenomics and Comparative Genomic Analyses: Description of Robertmurraya Kyonggiensis Sp. Nov. and Proposal for an Emended Genus Bacillus Limiting It …. *Int. J. Syst. Evol. Microbiol.* **2020**, *70*, 5753–5798, doi:10.1099/ijsem.0.004475.
41. AOAC981_12—PDFCOFFEE.COM Available online: https://pdfcoffee.com/aoac98112-pdf-free.html (accessed on 19 March 2026).
42. Miller, G.L. Use of Dinitrosalicylic Acid Reagent for Determination of Reducing Sugar. *Anal. Chem.* **2002**, *31*, 426–428, doi:10.1021/ac60147a030.
43. Trinder, P. Determination of Blood Glucose Using an Oxidase-Peroxidase System with a Non-Carcinogenic Chromogen. *J. Clin. Pathol.* **1969**, *22*, 158–161, doi:10.1136/jcp.22.2.158.
44. Pérez Rivero, C.; Sun, C.; Theodoropoulos, C.; Webb, C. Polyhydroxyalkanoates Production from Laboratory to Industrial Scale: A Review. *Int. J. Biol. Macromol.* **2025**, *310*, 143255, doi:10.1016/j.bej.2016.04.016.
45. Shahid, S.; Mosrati, R.; Corroler, D.; Amiel, C.; Gaillard, J.L. Bioconversion of Glycerol into Polyhydroxyalkanoates through an Atypical Metabolism Shift Using Priestia Megaterium during Fermentation Processes: A Statistical Analysis of Carbon and Nitrogen Source Concentrations. *Int. J. Biol. Macromol.* **2024**, *256*, 128116, doi:10.1016/j.ijbiomac.2023.128116.
46. Abid, S.; Raza, Z.A.; Hussain, T. Production Kinetics of Polyhydroxyalkanoates by Using Pseudomonas Aeruginosa Gamma Ray Mutant Strain EBN-8 Cultured on Soybean Oil. *3 Biotech 2016 6:2* **2016**, *6*, 142-, doi:10.1007/s13205-016-0452-4.
47. Hong, K.; Sun, S.; Tian, W.; Chen, G.Q.; Huang, W. A Rapid Method for Detecting Bacterial Polyhydroxyalkanoates in Intact Cells by Fourier Transform Infrared Spectroscopy. *Appl. Microbiol. Biotechnol.* **1999**, *51*, 523–526, doi:10.1007/s002530051427.
48. Randriamanhefa, S.; Renard, E.; Guérin, P.; Langlois, V. Fourier Transform Infrared Spectroscopy for Screening and Quantifying Production of PHAs by Pseudomonas Grown on Sodium Octanoate. *Biomacromolecules* **2003**, *4*, 1092–1097, doi:10.1021/bm034104o.
49. STAR e Software for Windows ® 2000 and Windows ® XP METTLER TOLEDO STAR e Thermal Analysis System User Handbook.

 doi:10.20944/preprints202603.2393.v1

50. Muneer, F.; Rasul, I.; Azeem, F.; Siddique, M.H.; Zubair, M.; Nadeem, H. Microbial Polyhydroxyalkanoates (PHAs): Efficient Replacement of Synthetic Polymers. *Journal of Polymers and the Environment 2020 28:9* **2020**, *28*, 2301–2323, doi:10.1007/s10924-020-01772-1.
51. Getino, L.; Martín, J.L.; Chamizo-Ampudia, A. A Review of Polyhydroxyalkanoates: Characterization, Production, and Application from Waste. *Microorganisms 2024, Vol. 12,* **2024**, *12*, doi:10.3390/microorganisms12102028.
52. Myers H Raymond, M.C.D.& A.-C.C.C. Response Surface Methodology: Process and Product Optimization Using ... -. *Wiley Series in Probability And Statistics, 4th ed., John Wiley & Sons Inc., New Jersey* **2016**, 894.
53. Derringer, G.; Suich, R. Simultaneous Optimization of Several Response Variables. *Journal of Quality Technology* **1980**, *12*, 214–219, doi:10.1080/00224065.1980.11980968.
54. De Vuyst, L.; Weckx, S. The Cocoa Bean Fermentation Process: From Ecosystem Analysis to Starter Culture Development. *J. Appl. Microbiol.* **2016**, *121*, 5–17, doi:10.1111/jam.13045.
55. Mota-Gutierrez, J.; Botta, C.; Ferrocino, I.; Giordano, M.; Bertolino, M.; Dolci, P.; Cannoni, M.; Cocolin, L. Dynamics and Biodiversity of Bacterial and Yeast Communities during Fermentation of Cocoa Beans. *Appl. Environ. Microbiol.* **2018**, *84*, doi:10.1128/AEM.01164-18.
56. Systematic Bacteriology. *Systematic Bacteriology* **2009**, doi:10.1007/978-0-387-68489-5.
57. Thamarai, P.; Vickram, A.S.; Saravanan, A.; Deivayanai, V.C.; Evangeline, S. Recent Advancements in Biosynthesis, Industrial Production, and Environmental Applications of Polyhydroxyalkanoates (PHAs): A Review. *Bioresour. Technol. Rep.* **2024**, *27*, 101957, doi:10.1016/j.biteb.2024.101957.
58. Koller, M.; Mukherjee, A. A New Wave of Industrialization of PHA Biopolyesters. *Bioengineering 2022, Vol. 9,* **2022**, *9*, doi:10.3390/bioengineering9020074.
59. Sachan, R.S.K.; Devgon, I.; Karnwal, A.; Mahmoud, A.E.D. Valorization of Sugar Extracted from Wheat Straw for Eco-Friendly Polyhydroxyalkanoate (PHA) Production by Bacillus Megaterium MTCC 453. *Bioresour. Technol. Rep.* **2024**, *25*, 101770, doi:10.1016/j.biteb.2024.101770.
60. Balakrishna Pillai, A.; Jaya Kumar, A.; Thulasi, K.; Kumarapillai, H. Evaluation of Short-Chain-Length Polyhydroxyalkanoate Accumulation in Bacillus Aryabhattai. *Brazilian Journal of Microbiology* **2017**, *48*, 451–460, doi:10.1016/j.bjm.2017.01.005.
61. Kim, M.; Oh, H.S.; Park, S.C.; Chun, J. Towards a Taxonomic Coherence between Average Nucleotide Identity and 16S RRNA Gene Sequence Similarity for Species Demarcation of Prokaryotes. *Int. J. Syst. Evol. Microbiol.* **2014**, *64*, 346–351, doi:10.1099/ijs.0.059774-0.
62. Shivaji, S.; Chaturvedi, P.; Begum, Z.; Pindi, P.K.; Manorama, R.; Padmanaban, D.A.; Shouche, Y.S.; Pawar, S.; Vaishampayan, P.; Dutt, C.B.S.; et al. Janibacter Hoylei Sp. Nov., Bacillus Isronensis Sp. Nov. and Bacillus Aryabhattai Sp. Nov., Isolated from Cryotubes Used for Collecting Air from the Upper Atmosphere. *Int. J. Syst. Evol. Microbiol.* **2009**, *59*, 2977–2986, doi:10.1099/ijs.0.002527-0.
63. Spence, S.; Uchida, A.; Aung, N.W.; Dacanay, J.G.A.; Lim, S.B.Y.; Drautz-Moses, D.I.; Schuster, S.C.; Kim, H.L. Comparative Genome Analysis Using Whole Genome Sequences Suggests Ongoing Speciation between Priestia Aryabhattai and Priestia Megaterium. *Front. Ecol. Evol.* **2026**, *14*, 1777162, doi:10.3389/fevo.2026.1777162.
64. Mousavi, S.S.; Karami, A.; Saharkhiz, M.J.; Etemadi, M.; Ravanbakhsh, M. Microbial Amelioration of Salinity Stress in Endangered Accessions of Iranian Licorice (Glycyrrhiza Glabra L.). *BMC Plant Biology 2022 22:1* **2022**, *22*, 322-, doi:10.1186/s12870-022-03703-9.
65. Park, Y.G.; Mun, B.G.; Kang, S.M.; Hussain, A.; Shahzad, R.; Seo, C.W.; Kim, A.Y.; Lee, S.U.; Oh, K.Y.; Lee, D.Y.; et al. Bacillus Aryabhattai SRB02 Tolerates Oxidative and Nitrosative Stress and Promotes the Growth of Soybean by Modulating the Production of Phytohormones. *PLoS One* **2017**, *12*, e0173203, doi:10.1371/journal.pone.0173203.
66. Ortiz-Valbuena, K.L.; Álvarez-León, R. Efecto Del Vertimiento de Subproductos Del Beneficio de Cacao (Theobroma Cacao L.) Sobre Algunas Propiedades Químicas y Biológicas En Los Suelos de Una Finca Cacaotera, Municipio de Yaguará (Huila, Colombia). *Boletín Científico Centro de Museos, Museo de Historia Natural* **2015**, *19*, 65–84, doi:10.17151/bccm.2015.19.1.5.
67. Wacher-Rodarte, M.-C. Microorganismos y Chocolate. *Revista Digital Universitaria* **2011**, *12*, 1–9.

 doi:10.20944/preprints202603.2393.v1

68. Alava-Zambrano, W.-A. Caracterización Física–Química Del Mucílago de Cacao (Theobroma Cacao L.) Con Énfasis En Los Azúcares Que Lo Componen. Magister en Procesamiento de Alimentos, Universidad Agraria del Ecuador: Guayaquil, 2020.
69. AOAC Official Method 996.06Fat (Total, Saturated, and Unsaturated) in Foods: Hydrolytic Extraction Gas Chromatographic Method. *Official Methods of Analysis of AOAC INTERNATIONAL* **2023**, doi:10.1093/9780197610145.003.3515.
70. 08 Total Ash Methods Available online: https://www.cerealsgrains.org/resources/Methods/Pages/08TotalAsh.aspx (accessed on 21 March 2026).
71. Sharma, D.; Chetri, P.B.; Ranga, V.; Sen, S.; Sarmah, B.K.; Barooah, M. Genomic Analysis of Acid Tolerance Genes and Deciphering the Function of YdaG Gene in Mitigating Acid Tolerance in Priestia Megaterium. *Front. Microbiol.* **2024**, *15*, 1414777, doi:10.3389/fmicb.2024.1414777.
72. Arriaga, M.; Pinar, F.J.; Izarra, I.; Amo, J. del; Vicente, J.; Fernández-Morales, F.J.; Mena, J. Valorization of Agri-Food Waste into PHA and Bioplastics: From Waste Selection to Transformation. *Applied Sciences (Switzerland)* **2025**, *15*, doi:10.3390/APP15031008.
73. Balakrishna Pillai, A.; Jaya Kumar, A.; Kumarapillai, H. Enhanced Production of Poly(3-Hydroxybutyrate) in Recombinant Escherichia Coli and EDTA–Microwave-Assisted Cell Lysis for Polymer Recovery. *AMB Express 2018 8:1* **2018**, *8*, 142-, doi:10.1186/s13568-018-0672-6.
74. Muneer, F.; Rasul, I.; Azeem, F.; Siddique, M.H.; Zubair, M.; Nadeem, H. Microbial Polyhydroxyalkanoates (PHAs): Efficient Replacement of Synthetic Polymers. *Journal of Polymers and the Environment 2020 28:9* **2020**, *28*, 2301–2323, doi:10.1007/s10924-020-01772-1.
75. Saravanan, K.; Umesh, M.; Kathirvel, P. Microbial Polyhydroxyalkanoates (PHAs): A Review on Biosynthesis, Properties, Fermentation Strategies and Its Prospective Applications for Sustainable Future. *Journal of Polymers and the Environment 2022 30:12* **2022**, *30*, 4903–4935, doi:10.1007/s10924-022-02562-7.
76. Seabold, S.; Perktold, J. Statsmodels: Econometric and Statistical Modeling with Python. *SciPy 2010* **2010**, 92–96, doi:10.25080/majora-92bf1922-011.
77. Myers, R.; Montgomery, D.; Anderson-Cook, C. *Response Surface Methodology: Process and Product Optimization Using Designed Experiments*; 4th ed.; John Wiley & Sons, Inc: Hoboken, New Jersey, 2016; ISBN 978-1-118-91601-8.
78. Penkhrue, W.; Jendrossek, D.; Khanongnuch, C.; Pathomareeid, W.; Aizawa, T.; Behrens, R.L.; Lumyongid, S. Response Surface Method for Polyhydroxybutyrate (PHB) Bioplastic Accumulation in Bacillus Drentensis BP17 Using Pineapple Peel. *PLoS One* **2020**, *15*, e0230443, doi:10.1371/journal.pone.0230443.
79. Muneer, F.; Rasul, I.; Qasim, M.; Sajid, A.; Nadeem, H. Optimization, Production and Characterization of Polyhydroxyalkanoate (PHA) from Indigenously Isolated Novel Bacteria. *Journal of Polymers and the Environment 2022 30:8* **2022**, *30*, 3523–3533, doi:10.1007/s10924-022-02444-y.
80. Virtanen, P.; Gommers, R.; Oliphant, T.E.; Haberland, M.; Reddy, T.; Cournapeau, D.; Burovski, E.; Peterson, P.; Weckesser, W.; Bright, J.; et al. SciPy 1.0: Fundamental Algorithms for Scientific Computing in Python. *Nature Methods 2020 17:3* **2020**, *17*, 261–272, doi:10.1038/s41592-019-0686-2.
81. Arumugam, A.; Anudakshaini, T.S.; Shruthi, R.; Jeyavishnu, K.; Sundarra Harini, S.; Sharad, J.S. Low-Cost Production of PHA Using Cashew Apple (Anacardium Occidentale L.) Juice as Potential Substrate: Optimization and Characterization. *Biomass Convers. Biorefin.* **2020**, *10*, 1–12, doi:10.1007/s13399-019-00502-5.
82. Apati, G.P.; Kelbert, M.; Sombrio, B.R.; Schneider, A.L. dos S.; Garcia, M.C.F.; Furigo Junior, A.; Pezzin, A.P.T. Evaluation of the Addition of Glycerol to Cupriavidus Necator Culture Medium over Poly(3-Hydroxybutyrate) Production. *Matéria (Rio de Janeiro)* **2017**, *22*, doi:10.1590/s1517-707620170005.0243.
83. Możejko-Ciesielska, J.; Pokoj, T. Exploring Nutrient Limitation for Polyhydroxyalkanoates Synthesis by Newly Isolated Strains of Aeromonas Sp. Using Biodiesel-Derived Glycerol as a Substrate. *PeerJ* **2018**, *2018*, e5838, doi:10.7717/peerj.5838.
84. Fernandez, E.R.; Concha, J.L.H.; Sánchez, S.A.M. Producción De Polihidroxialcanoatos (Phas) A Partir De Ralstonia Eutropha En Un Medio Con Harina De Yuca Como Fuente De Carbono. *Biotecnología en el Sector Agropecuario y Agroindustrial* **2016**, *14*, 19–26, doi:10.18684/bsaa(14)19-26.

 doi:10.20944/preprints202603.2393.v1

85. Porwal, S.; Kumar, T.; Lal, S.; Rani, A.; Kumar, S.; Cheema, S.; Purohit, H.J.; Sharma, R.; Singh Patel, S.K.; Kalia, V.C. Hydrogen and Polyhydroxybutyrate Producing Abilities of Microbes from Diverse Habitats by Dark Fermentative Process. *Bioresour. Technol.* **2008**, *99*, 5444–5451, doi:10.1016/j.biortech.2007.11.011.
86. Bhola, S.; Arora, K.; Kulshrestha, S.; Mehariya, S.; Bhatia, R.K.; Kaur, P.; Kumar, P. Established and Emerging Producers of PHA: Redefining the Possibility. *Applied Biochemistry and Biotechnology 2021 193:11* **2021**, *193*, 3812–3854, doi:10.1007/s12010-021-03626-5.
87. Ridella, F.; Fernández, E.; Álvarez-García, S.; Marcet, I.; Rendueles, M.; Díaz, M. Polyhydroxyalkanoates Production from Cocoa Bean Shell Fat: Bioprocess Optimization and Polymer Characterization. *Int. J. Biol. Macromol.* **2025**, *331*, doi:10.1016/j.ijbiomac.2025.148407.
88. Ramos, L.H.; Cisneros-Yupanqui, M.; Santisteban Soto, D.V.; Lante, A.; Favaro, L.; Casella, S.; Basaglia, M. Exploitation of Cocoa Pod Residues for the Production of Antioxidants, Polyhydroxyalkanoates, and Ethanol. *Fermentation* **2023**, *9*, doi:10.3390/fermentation9090843.
89. R Wan Abdul Razak, W.; J Mohamad Yusuf, N.; Abdul-Aziz, A.; K Navaratnam, S.; Zubir, I.; E Rizlan Ross, E. Screening and Isolation of Polyhydroxyalkanoates (PHA)-Producing Bacteria from Landfill by Using Cocoa Pod Husks as Carbon Source. *International Journal of Engineering & Technology* **2019**, *7*, doi:10.14419/ijet.v7i4.14.27470.
90. Zheng, J.; Suh, S. Strategies to Reduce the Global Carbon Footprint of Plastics. *Nature Climate Change 2019 9:5* **2019**, *9*, 374–378, doi:10.1038/s41558-019-0459-z.
91. Randriamanhefa, S.; Renard, E.; Guérin, P.; Langlois, V. Fourier Transform Infrared Spectroscopy for Screening and Quantifying Production of PHAs by Pseudomonas Grown on Sodium Octanoate. *Biomacromolecules* **2003**, *4*, 1092–1097, doi:10.1021/bm034104o.
92. Bunaciu, A.A.; Aboul-Enein, H.Y.; Hoang, V.D. Vibrational Spectroscopy Applications in Biomedical, Pharmaceutical and Food Sciences. *Vibrational Spectroscopy Applications in Biomedical, Pharmaceutical and Food Sciences* **2020**, doi:10.1016/c2018-0-04768-4.
93. Bloembergen, S.; Holden, D.A.; Hamer, G.K.; Bluhm, T.L.; Marchessault, R.H. Studies of Composition and Crystallinity of Bacterial Poly(β-Hydroxybutyrate-Co-β-Hydroxyvalerate). *Macromolecules* **2002**, *19*, 2865–2871, doi:10.1021/ma00165a034.
94. Xu, J.; Guo, B.H.; Yang, R.; Wu, Q.; Chen, G.Q.; Zhang, Z.M. In Situ FTIR Study on Melting and Crystallization of Polyhydroxyalkanoates. *Polymer (Guildf).* **2002**, *43*, 6893–6899, doi:10.1016/S0032-3861(02)00615-8.
95. Sato, H.; Murakami, R.; Padermshoke, A.; Hirose, F.; Senda, K.; Noda, I.; Ozaki, Y. Infrared Spectroscopy Studies of CH···O Hydrogen Bondings and Thermal Behavior of Biodegradable Poly(Hydroxyalkanoate). *Macromolecules* **2004**, *37*, 7203–7213, doi:10.1021/ma049117o.
96. Penkhrue, W.; Jendrossek, D.; Khanongnuch, C.; Pathomareeid, W.; Aizawa, T.; Behrens, R.L.; Lumyongid, S. Response Surface Method for Polyhydroxybutyrate (PHB) Bioplastic Accumulation in Bacillus Drentensis BP17 Using Pineapple Peel. *PLoS One* **2020**, *15*, e0230443, doi:10.1371/journal.pone.0230443.
97. Muneer, F.; Rasul, I.; Qasim, M.; Sajid, A.; Nadeem, H. Optimization, Production and Characterization of Polyhydroxyalkanoate (PHA) from Indigenously Isolated Novel Bacteria. *J. Polym. Environ.* **2022**, *30*, 3523–3533, doi:10.1007/s10924-022-02444-y.
98. Tanikkul, P.; Sullivan, G.L.; Sarp, S.; Pisutpaisal, N. Biosynthesis of Medium Chain Length Polyhydroxyalkanoates (Mcl-PHAs) from Palm Oil. *Case Studies in Chemical and Environmental Engineering* **2020**, *2*, 100045, doi:10.1016/j.cscee.2020.100045.
99. Barham, P.J.; Keller, A.; Otun, E.L.; Holmes, P.A. Crystallization and Morphology of a Bacterial Thermoplastic: Poly-3-Hydroxybutyrate. *J. Mater. Sci.* **1984**, *19*, 2781–2794, doi:10.1007/BF01026954.
100. Raza, Z.A.; Abid, S.; Banat, I.M. Polyhydroxyalkanoates: Characteristics, Production, Recent Developments and Applications. *Int. Biodeterior. Biodegradation* **2018**, *126*, 45–56, doi:10.1016/j.ibiod.2017.10.001.
101. Gunaratne, L.M.W.K.; Shanks, R.A. Multiple Melting Behaviour of Poly(3-Hydroxybutyrate-Co-Hydroxyvalerate) Using Step-Scan DSC. *Eur. Polym. J.* **2005**, *41*, 2980–2988, doi:10.1016/j.eurpolymj.2005.06.015.

 doi:10.20944/preprints202603.2393.v1

102. Righetti, M.C.; Tombari, E.; Di Lorenzo, M.L. The Role of the Crystallization Temperature on the Nanophase Structure Evolution of Poly[(R)-3-Hydroxybutyrate]. *Journal of Physical Chemistry B* **2013**, *117*, 12303–12311, doi:10.1021/jp4063127.
103. Lenz, R.W.; Marchessault, R.H. Bacterial Polyesters: Biosynthesis, Biodegradable Plastics and Biotechnology. *Biomacromolecules* **2004**, *6*, 1–8, doi:10.1021/bm049700c.
104. Ariffin, H.; Nishida, H.; Shirai, Y.; Hassan, M.A. Determination of Multiple Thermal Degradation Mechanisms of Poly(3-Hydroxybutyrate). *Polym. Degrad. Stab.* **2008**, *93*, 1433–1439, doi:10.1016/j.polymdegradstab.2008.05.020.
105. Kopinke, F.D.; Remmler, M.; Mackenzie, K. Thermal Decomposition of Biodegradable Polyesters—I: Poly(β-Hydroxybutyric Acid). *Polym. Degrad. Stab.* **1996**, *52*, 25–38, doi:10.1016/0141-3910(95)00221-9.
106. Penkhrue, W.; Jendrossek, D.; Khanongnuch, C.; Pathomareeid, W.; Aizawa, T.; Behrens, R.L.; Lumyongid, S. Response Surface Method for Polyhydroxybutyrate (PHB) Bioplastic Accumulation in Bacillus Drentensis BP17 Using Pineapple Peel. *PLoS One* **2020**, *15*, e0230443, doi:10.1371/journal.pone.0230443.